Published in final edited form as:
*Adv Drug Deliv Rev*. 2019 January 01; 138: 302–325. doi:10.1016/j.addr.2019.01.005.

# Iron Oxide Nanoparticles: Diagnostic, Therapeutic and Theranostic Applications

**Seyed Mohammadali Dadfar**[#1], **Karolin Roemhild**[#1,2], **Natascha I. Drude**[1,3,4], **Saskia von Stillfried**[2], **Ruth Knüchel**[2], **Fabian Kiessling**[1], **Twan Lammers**[1,5,6,*]

[1]Department of Nanomedicine and Theranostics, Institute for Experimental Molecular Imaging, RWTH Aachen University Clinic, Aachen, Germany [2]Institute of Pathology, Medical Faculty RWTH Aachen University, Aachen, Germany [3]Department of Nuclear Medicine, RWTH Aachen University Clinic, Aachen, Germany [4]Leibniz Institute for Interactive Materials – DWI, RWTH Aachen University, Aachen, Germany [5]Department of Pharmaceutics, Utrecht University, Utrecht, The Netherlands [6]Department of Targeted Therapeutics, University of Twente, Enschede, The Netherlands

[#] These authors contributed equally to this work.

## Abstract

Many different iron oxide nanoparticles have been evaluated over the years, for many different biomedical applications. We here summarize the synthesis, surface functionalization and characterization of iron oxide nanoparticles, as well as their (pre-) clinical use in diagnostic, therapeutic and theranostic settings. Diagnostic applications include liver, lymph node, inflammation and vascular imaging, employing mostly magnetic resonance imaging but recently also magnetic particle imaging. Therapeutic applications encompass iron supplementation in anemia and advanced cancer treatments, such as modulation of macrophage polarization, magnetic fluid hyperthermia and magnetic drug targeting. Because of their properties, iron oxide nanoparticles are particularly useful for theranostic purposes. Examples of such setups, in which diagnosis and therapy are intimately combined and in which iron oxide nanoparticles are used, are image-guided drug delivery, image-guided and microbubble-mediated opening of the blood-brain barrier, and theranostic tissue engineering. Together, these directions highlight the versatility and the broad applicability of iron oxide nanoparticles, and they indicate that multiple iron oxide nanoparticle-based materials will be integrated in future medical practice.

### Keywords

SPION; USPIO; MRI; MPI; MFH; Nanomedicine; Theranostics

[*]Corresponding author (tlammers@ukaachen.de).


Europe PMC Funders Author Manuscripts

# 1 Introduction

Iron oxide nanoparticles, which belong to the ferrimagnetic class of magnetic materials, are used for a wide variety of biomedical and bioengineering applications [1, 2]. Among the different types of iron oxide-based nanoparticles are magnetite ($Fe_3O_4$), maghemite (y-$Fe_2O_3$) and mixed ferrites ($MFe_2O_4$ where M = Co, Mn, Ni or Zn) [3]. Upon surface-modification, the resulting superparamagnetic iron oxide nanoparticles (SPION) can be employed for magnetic resonance imaging (MRI) [4–8], magnetic particle imaging (MPI) [9–12], targeted delivery of drugs, proteins, antibodies, and nucleic acids [6, 7, 13, 14], hyperthermia [15–17], biosensing [18], tissue repair [19], and separation of biomolecules [20]. This widespread list of applications not only results from the magnetic properties of SPION, but also from the fact that they can be synthesized in different sizes and shapes. SPION have high magnetic moments when exposed to an external magnetic field, and no remaining magnetic moment when the magnetic field is turned off [21]. Many iron oxide nanoparticles have been evaluated in preclinical and clinical trials, and several of them have reached the market (Table 1) [4, 22–26]. However, some of the approved SPION have later on been withdrawn, because of the availability of alternative diagnostic probes and protocols [27].

In this manuscript, we summarize synthetic protocols and characterization methods to obtain iron oxide nanoparticles with desired features, and we outline their most prominent (pre-) clinical applications. In the first part, the most frequently used preparation techniques are summarized. We focus on those synthesis routes which cover about 90% of all synthesis techniques and which have advantages such as simplicity, low cost and high reproducibility. We also discuss the most common surface modification strategies, which are necessary to optimally exploit their specific properties and causes usefulness for biomedical applications [28]. The second part of our review provides an overview of SPION formulations currently used in the clinic for diagnostic, therapeutic and theranostic purposes. We summarize selected preclinical and clinical studies conducted in these areas of research, and we discuss strategies to expand the use and the usefulness of iron oxide nanoparticles in future biomedical settings.

# 2 Synthesis, surface modification, characterization and toxicity of iron oxide nanoparticles

## 2.1 Synthesis methods

The magnetic properties of iron oxide nanoparticles depend on their composition and morphology. Thus, the synthetic method needs to be carefully selected, ensuring control over shape, size, size distribution and crystallinity of the particles. SPION can be produced in several different ways, encompassing chemical, physical and biosynthetic methodologies [3, 25, 28, 29]. Chemical approaches are employed in the vast majority of cases. Physical methods, which include powder ball milling, electron beam lithography, aerosol and gas phase deposition suffer from the lack of ability to control the size of particles in the nanometer size range [29]. Biological methods rely on reduction-oxidation reactions, in which microbial enzymes or plant phytochemicals are responsible for the reduction of salts

into SPION. Such biosynthetic routes are generally considered eco-friendly (green chemistry) and the products obtained using such procedures tend to show good biocompatibility. However, the yield of such methods is low and the size distribution is broad. Together, physical and biosynthetic synthesis protocols make up for less than 10% of all SPION synthesis methods [3]. In the following paragraphs, we therefore only focus on commonly employed chemical synthesis routes (see Figure 1 and Table 2).

**2.1.1 Co-precipitation—**The co-precipitation technique, which is among the most simple and efficient synthesis procedures, is based on simultaneous precipitation of $Fe^{2+}$ and $Fe^{3+}$ aqueous salt solutions via the addition of a weak or strong base. Most of commercially available SPION are synthesized via this method. Many synthetic parameters influence the size, shape and composition of the eventually obtained iron oxide nanoparticles, e.g. $Fe^{2}$+/ $Fe^{3}$+ ratio, temperature, pH, type of salt used (chloride, nitrate, sulfate, perchlorate), and type of base used (NaOH, $NH_4OH$, $Na_2CO_3$). While the co-precipitation technique is one of the most cost-effective routes for the high-yield synthesis of SPION with appropriate magnetic properties, the nanoparticles generated via this method usually exhibit a low degree of crystallinity and a relatively large polydispersity. To – at least in part – overcome these drawbacks, several modified versions of the co-precipitation technique have been developed [30–32]. These for instance include preparation of Fe3O4 nanoparticles under a static magnetic field [33], assistance of ultrasound [34], using alkanolamines as base [35], *in situ* co-precipitation in a carboxyl-functionalized polymer matrix [36], and finally co-precipitation of $FeCl_3.6H_2O$, $FeSO_4.7H_2O$, and $Gd(NO_3)_3$ aqueous solutions by addition of NaOH [37].

**2.1.2 Thermal decomposition—**SPION with high control over size and shape, narrow size distribution and good crystallinity can be prepared via thermal decomposition of organoiron precursors in high-boiling point organic solvents in the presence of stabilizing surfactants [38, 39]. Amphiphilic surfactants like oleic acid, oleylamine, fatty acids and hexadecylamine allow adjustment of the nucleation and growth kinetics of the nanoparticles. On the one hand, the high reaction temperatures and the presence of the surfactant in the medium result in high quality samples in terms of size dispersion and crystallinity. On the other hand, however, this method is not very environmentally friendly, due to the use of toxic chemicals, such as chloroform, hexane and iron pentacarbonyl in the synthesis. Furthermore, because of the presence of a hydrophobic coating on the surface of the magnetic nanoparticles, an additional surface modification step is needed to obtain water-dispersible and biocompatible nanoparticles that are useful for biomedical applications. When employing the thermal decomposition method to prepare SPION, control over morphology and nanoparticle size strongly depends on the reaction time, the reaction temperature and the precursor-to-surfactant ratio [40].

**2.1.3 Microemulsion—**Microemulsion systems are thermodynamically stable isotropic dispersion of two immiscible liquids. Microemulsions can essentially be subdivided in two categories: oil-in-water (o/w; normal micelles) and water-in-oil (w/o; reversed micelles). The dispersed phase typically serves as a nano/micro-reactor, proving a confined environment for the nucleation and controlled growth of nano- and microparticles. Several

kinds of amphiphilic surfactants, like dioctyl sodium sulfosuccinate (DSS), cetyltrimethylammonium bromide (CTAB), sodium dodecylsulfate (SDS) and polyethoxylates (e.g. Tween-20 and -80) are used for the formation of micellar microemulsion systems [30]. The main advantage of employing microemulsion methodology to prepare SPION is that the nanoparticle size can be controlled by varying the size of the micelles. Moreover, due to the relatively homogenous size of the micelles, an improvement in the polydispersity of the particles is observed. Drawbacks of microemulsion synthesis include the fact the limited reaction temperature that can typically be achieved result in SPION with low crystallinity and in low yield. Maintenance of micelle structure at high reaction temperature [41] or thermal annealing of synthesized iron oxide [42] are ways to increase the crystallinity of the particles prepared by this method. Difficulties related to scale-up and unfavorable effects of residual surfactants on the properties of the iron oxide particles are additional disadvantages of the microemulsion method [28].

**2.1.4 Sol-gel—**The sol–gel technique, which is commonly employed for production of silica-coated SPION, is based on the formation of colloidal sols using hydrolysis and condensation of tetraethyl orthosilicate (TEOS) in ethanol and 30% aqueous $H_2O_2$ with Fe (III) solutions. The sol is then gelled by chemical reaction or solvent removal, to obtain a 3D iron oxide network. To get iron oxide nanoparticles, the formed gel requires an additional crushing step after drying and solvent removal. Adding surfactant prior to gelation results in a decrease in the free energy of the system and consequently leads to the formation of nano-sized iron oxides without the formation of a 3D network. The sol-gel synthesis technique provides a straightforward method to synthesize relatively monodisperse and relatively larged-sized nanoparticles, in relatively high yields, at ambient conditions. However, since the sol–gel technique is performed at room temperature, further heat treatment is needed to obtain the desired crystalline structures. The method also comes with by-product contaminations, and thus requires post-treatment for purification. Temperature, pH, the used solvent and the used concentration of salt precursors are parameters that influence the structure and the properties of the SPION gel. The thickness of the silica shell is typically tuned by controlling the amount of TEOS and ammonia [43–45].

**2.1.5 Additional chemical methods—**Besides the above synthetic strategies, there are several other chemical routes for synthesizing SPION, including hydrothermal, sonochemical and electrochemical deposition methodologies. Advantages of the hydrothermal method are its low cost and the relatively large-scale production of highly crystalline iron oxide nanoparticles. In this method, a mixture of iron salts dissolved in aqueous solution is placed into a sealed teflon-lined stainless-steel autoclave, in which the temperature can be raised above 200 °C. As a result of this, the reaction pressure is raised beyond atmospheric pressure. The synergistic effect of high temperature and high pressure leads to an improvement in the quality of the nanocrystals and their magnetic properties. Control over nanoparticle formation, size and size distribution can be achieved by varying process parameters such as temperature, pressure, precursor concentration and reaction time. However, it is difficult to control the final size of particles and most of the times polydisperse samples are obtained under hydrothermal conditions [3, 28, 46].

Progress in the synthesis of bare or functionalized SPION has recently been made via the use of sonochemical decomposition of organoiron precursors. In this process, the high energy of ultrasonic irradiation creates acoustic cavitations in the aqueous medium which provide local heat with a temperature of around 5000 °C. This method provides monodisperse SPION with a variety of shapes under ambient conditions (usually in the presence of air) and without the need of high bulk temperatures or long reaction times. In general, thermally-induced processes result in crystalline nanoparticles. However, in the ultrasonic-driven method, the huge cooling rate of cavitations during quenching prevents the crystallization of SPION. Thus, the obtained amorphous SPION need to be further processed by heat-treatment after they have been synthesized [3, 28, 46–48].

Electrochemical deposition has also been used to synthesize maghemite and magnetite SPION. In electrochemical synthesis, an electric current is passed between two electrodes (i.e. the anode and the cathode) located in an electrolyte. In this technique, the anode is first oxidized to create metal ion species in solution, and then the metal ions are reduced to metal by the cathode. This has to be done in the presence of a stabilizer, which acts as a coating. The product is obtained with high purity and the control of particle size is achieved by tuning the voltage or the current applied to the system. The distance between electrodes is important in the successful synthesis of SPION. This method does not require high temperatures. This technique has some disadvantages, including e.g. the fact that it is not yet useful for large-scale synthesis. Also, since reactions are usually performed at room temperature, the synthesized products often show some amorphous parts [3, 49].

## 2.2 Surface modification of iron oxide nanoparticles

The surface of iron oxide nanoparticles is, either during or after preparation, typically modified with a biocompatible coating. This is done to stabilize the SPION in biological media, to prevent them from possible oxidation, to improve their biocompatibility, and/or to attach functional molecules such as targeting ligands or drugs.

Prototypic examples of materials used to coat iron oxide nanoparticles are polymers [28, 47, 50], fatty acids (like oleic acid, stearic acid, lauric acid and dodecylphosphonic acid) [51–55], amino acids (like phenyl alanine, tyrosine, arginine, lysine and cysteine) [56–58],_metals (like gold, gadolinium and silver) [59–61] and oxides (like silica and $TiO_2$) [62–64]. Among these materials, polymers are arguably the most popular coating materials. Over the recent years several natural and synthetic polymers, such as dextran [31, 65, 66], gelatin [67], alginate [68, 69], chitosan [69, 70], starch [71], albumin [72, 73], casein [74], poly (ethylene glycol) (PEG) [75–78], poly (vinyl pyrrolidone) (PVP) [79], poly (vinyl alcohol) (PVA) [80], polydopamine [81, 82], poly (lactic-co-glycolic acid) (PLGA) [83] and dendrimers [84] have been used to coat different forms of SPION. Some examples of polymeric coatings are presented in Figure 2.

Among the different polymer coatings, PEG and dextran are the most extensively employed ones, likely because they are generally regarded as safe (GRAS), and also because they are not very rapidly recognized by macrophages in liver and spleen when administered intravenously [85, 86]. PEG $(C_2H_4O)_n$ and PEGylated coatings like PEGylated starch (coating agent in feruglose) are highly biocompatible and often used to prolong vascular

circulation of nanoparticles like SPION. Molecular weight and surface density of PEG coatings are two critical parameters that influence the dispersion stability, cytotoxicity and blood circulation time of iron oxide nanoparticles [71, 87]. Similarly, dextran $(C_6H_{10}O_5)_n$ (coating agent in ferumoxtran and ferumoxides) and its derivatives carboxydextran (coating agent in ferucarbotran) and carboxymethyl-dextran (coating agent in ferumoxytol) are also known to be highly biocompatible. It has to be kept in mind in this regard that while dextran has no direct cytotoxic effects, the degradation of the dextran shell may influence certain cellular processes [30, 65, 86, 87].

In addition to these standard polymers, many efforts have been invested in recent years in developing stimuli-responsive polymeric coatings. Stimuli-responsive polymers typically alter their swelling behavior and undergo a reversible phase transition in response to changes in environmental stimuli, such as temperature, pH, light, enzymes, ionic strength, electric field and magnetic field. Among these stimuli, temperature and pH have been employed most widely. Temperature-sensitive polymers exhibit lower critical solution temperature (LCST) and their physical and chemical properties change by causing the change in surrounding temperature. They are swollen in aqueous media when the temperature is below the LCST, and they undergo a phase transition when the temperature is increased above the LCST. For pH-sensitive polymeric coatings, their shapes and volumes change with the variation of external pH. Polymers having weakly acidic pendant groups for instance display pH responsiveness because of altered protonation of carboxyl groups. Figure 2 presents several prototypic examples of temperature- and pH-responsive polymers that are used to coat iron oxide nanoparticles [88–93].

Iron oxide nanoparticles can be entrapped inside of vesicles like liposomes [94–97] or polymeric micelles [98–101]. While the encapsulation of SPION in vesicles differs from the surface functionalization methods described, this method provide similar advantages, such as improvement of biocompatibility, improvement of in vivo performance and ability to attach functional molecules. Liposomes are amphiphilic phospholipids assembled in a bilayered hollow sphere structure. Hydrophilic SPION are located in the inner core of liposomes. Hydrophobic SPION are typically entrapped in the liposome bilayer. Liposomes encapsulating magnetite nanoparticles are known as magnetoliposomes (MLs) [94–97]. Polymeric micelles, i.e., self-assembled nanoparticles based on amphiphilic block copolymers, are core-shell materials in which the hydrophobic compartment is a suitable environment for the entrapment of hydrophobic SPION, while the hydrophilic shell helps to stabilize the nanoparticles in aqueous solution or biological media [98–102].

### 2.3 Characterization of iron oxide nanoparticles

Many different analytical techniques are employed to assess the physicochemical properties of iron oxide nanoparticles. Iron concentrations are typically determined by inductively coupled plasma mass spectroscopy (ICP-MS) or via the 1,10-phenanthroline assay. The flame atomic-absorption spectrometry (FAAS) technique is also used. Transmission electron microscopy (TEM) and atomic force microscopy (AFM) are powerful techniques to provide information on the core size, core size distribution and morphology of iron oxide nanoparticles [103, 104].

Selected area electron diffraction (SAED) pattern obtained from high-resolution TEM (HRTEM) is used to obtain information on the composition and crystallographic phase of crystalline SPION. As high-energy electrons pass through TEM specimens which are typically about 100 nm thick, they are treated as wave-like, rather than particle-like. The wavelength of high-energy electrons is a few thousandths, while the distance between atoms in the sample is about a hundred times higher. So, the atoms act as a diffraction grating to the electrons and some fraction of them will be scattered to particular angles, while another fraction continues to pass from the sample without deflection. Consequently, the image on the screen will be a series of spots where each spot corresponds to a satisfied diffraction condition for the crystal structure of sample [105]. X-Ray diffraction (XRD) is also frequently used to determine crystalline structure, and to calculate the crystalline size of SPION via the use of the Scherrer's equation. This equation relates the size of crystallites in a solid to the broadening of a peak in a diffraction pattern [106].

For determining the hydrodynamic diameter and the hydrodynamic size distribution of iron oxide nanoparticles, dynamic light scattering (DLS) and nanoparticle tracking analysis (NTA) are employed. Both techniques also allow monitoring of colloidal stability and aggregation behavior of nanoparticles in suspension. Although DLS is a powerful and readily accessible tool, it has several drawbacks. It for instance is very sensitive to the presence of large particles. NTA does not have this limitation and can be used for sizing particles from 30 nm to 1000 nm. In addition, NTA has a lower detection limit as compared to DLS [107].

Nuclear magnetic resonance spectroscopy (NMR), Fourier transform infrared spectroscopy (FT-IR) and X-ray photoelectron spectroscopy (XPS) analysis are performed to determine the surface characteristics of iron oxide nanoparticles and to verify the presence of certain desired functional groups. Size, size distribution and surface-to-volume ratio of iron oxide nanoparticles can be estimated based on the scattering intensity data obtained from small angle X-ray scattering (SAXS) or ultra-small angle X-ray scattering (USAXS). When employing these methodologies, nanoscale density differences are quantified via recording the elastic scattering behavior of X-rays when travelling through the material at small angles (depending on the angular range in which a clear scattering signal can be recorded, typically 0.1-10°) [108]. The magnetic properties of nanoparticles are typically studied by superconducting quantum interference measurement device (SQUID) measurements [103].

To investigate the usefulness of SPION for MR imaging, longitudinal (T1), transverse (T2), and effective transverse (T2*) relaxation times and their corresponding relaxation rates R1, R2, and R2* (which are the inverses of T1, T2, and T2*, respectively), are analyzed using MR scanners and nuclear magnetic resonance (NMR) spectroscopy. Via plotting the changes in R1 and R2 of MRI contrast agents as a function of their concentration, the corresponding relaxivities ($r_1$ and $r_2$) are determined, typically expressed in $mM^{-1}s^{-1}$. Different parameters like core size of SPION, shape, hydrodynamic diameter, size distribution, nanoparticles coating and aggregation influence the longitudinal and transverse relaxivities of iron oxide nanoparticles. While $r_2$ typically shows a linear increase with increasing the particle core size from 4-5 to 18 nm, $r_1$ remains rather invariant for particles larger than approximately 8 nm. Regarding the effect of hydrodynamic diameter and aggregation on relaxivities, $r_2$

gradually increases with the hydrodynamic diameter (up until approximately 80 nm) for small clusters, because SPION are consistently dispersed in water and protons diffuse between the magnetic cores. In the case of large clusters, if the size exceeds 90 nm, $r_2$ decreases with increasing size due to a reduction in the proton exchange rate arising from the reduction in surface accessibility. In addition to specifications of the contrast agent itself, relaxivity values depend on the applied magnetic field strength, temperature, and the substance in which the contrast agent is dispersed. For MRI contrast agents in clinical uses, it is common practice to refer to $r_1$ and $r_2$ values at 1.5 T, in serum or blood and at 37 °C (body temperature) [109–112].

On the basis of MPI measurements, the signal-to-noise ratio (SNR) as well as the full width at half maximum (FWHM) of the point spread function (PSF) in water, serum and whole blood are assessed. The SNR parameter expresses the ability of SPION to provide decent imaging capabilities in MPI. SNR is defined as the ratio of the power of sample signal to the power of background noise. Since different MPI tracers contain different amounts of iron, the SNR measured for a tracer needs to be normalized to the iron concentration. The PSF of SPION is a measure for the magnetization change as a function of the applied drive field. PSF is determined from spectroscopic MPI measurements using the method presented by Schmale et al. Based on the FWHM of the PSF, the spatial resolution (Δx) that is achievable in an MPI device is obtained. Spatial resolution depends linearly on the FWHM. Lower FWHM values refer to a higher achievable spatial resolution in MPI. As an important note, contrast generation in MPI critically depends on the parameters that affect the magnetization response like SPION size and size distribution [113, 114].

In order to evaluate hyperthermia performance, SPION can be exposed to radiofrequency, ultrasound, microwave or alternating magnetic field, and the specific absorption rate (SAR), which is a measure for the magnetic power absorbed per unit mass of magnetic material, is determined. The SAR depends on SPION size, monodispersity, structural and magnetic properties, and frequency and amplitude of the magnetic field. For commercially available SPION dispersions, SAR values are usually in the range between 4 and 100 W/g. Besides the structure and composition of the SPION, the frequency and the amplitude of the magnetic field applied during the measurements play important roles in heat generation and SAR. SAR increases by increasing either the amplitude or the frequency. Interestingly, Guardia *et al.* observed a linear SAR dependence as a function of frequency (at a fixed amplitude) and a quadratic SAR dependence as a function of amplitude (at a fixed frequency) for water-soluble iron oxide nanocubes [15, 115].

### 2.4 Analysis of the biocompatibility of SPION

The potential clinical applications of SPION call for careful assessment of their toxicological properties, especially if they are used for diagnostic purposes (which includes their use in healthy individuals). Therefore, every agent used in diagnostics needs to be extensively evaluated wwith regard to potential side effects. In general, enhanced iron levels are known to cause an increase of reactive oxygen species (ROS) via the Fenton reaction. Furthermore, if at the cellular level ROS production exceeds the cell's scavenging ability, lipid peroxidation and DNA damage can lead to cell death, via a process known as

ferroptosis [116]. Besides direct toxicity mediated by ROS, they are also known to be involved in redox regulation and in cellular signaling. In macrophages, ROS regulates cell death, proliferation, motility and phagocytic ability, and it is linked to an M1-like polarisation, which help to defend the body against bacteria and other pathogens [117, 118].

To assess the biocompatibility of SPION, several in vitro and in vivo setups have been employed. In vitro, upon prolonged incubation, surface-coated SPION are typically nontoxic at iron concentration up to and 10 μg/ml, while slight cytotoxicity is seen at 100 μg/ml. In general, SPION toxicity depends on a variety of factors, including - besides dosing and exposure time - also the nature of the coating material, the hydrodynamic diameter of the particle and SPION-protein interactions [119–122]. Certain coatings, such as polyethylenimine (PEI), have been claimed to show an activation of immunological pathways in vitro, as exemplified e.g. an M1-like activation of macrophages induced by PEI-coated SPION [123, 124]. Additionally, activation of dendritic cells has been observed upon exposure to poly(vinylalcohol)-coated SPION [125].

When loading cells with SPION for cell tracking purposes, care should be taken that labeling does not affect the proliferation, motility and function of the cells. Studies investigating the biological effects of (typically sugar-coated) SPION on dendritic cells [126], mesenchymal stem cells [127, 128], endothelial cells [129, 130] and tumor cells [131] have reported no impact on phenotype and cellular function. It is clear, however, that this strongly depends on loading dose, and that for each individual case, a compromise needs to be found, ensuring no effect of loaded SPION on cellular function on the one hand, and good in vivo detectability on the other hand.

Commonly used techniques to determine the in vitro cytotoxicity of SPION include the monitoring of mitochondrial redox activity via XTT or MTT assays, measuring lactate dehydrogenase (LDH) in the supernatant to assess cell membrane integrity, staining of immunochemistry markers characteristic for apoptosis and/or necrosis, and gene expression analysis. Such simple and straightforward in vitro toxicity assays provide a decent first impression of the biocompatibility of nanoparticle formulations. In vivo, aspects such as particle distribution, organ deposition and cellular accumulation also have to be considered. When administered intravenously, SPION typically accumulate in the liver and in the spleen, as these tissues have high vacularization, fenestrated blood vessels and high phagocytic capacity. These organs typically cope relatively well with high SPION accumulation, which can be explained – at least in part – by the fact that the liver is main storage organ for iron in the body [132]. As an intermediate model system, the zebrafish (Danio rerio) embryo assay has recently emerged as an interesting method for in vivo toxicity testing, enabling relatively high-throughput analyses in a system considerably more complex than cultured cells, but less expensive, less invasive and ethically less problematic than large-scale biocompatibility studies in mice or rats [133].

Several studies in patients have shown no (or only minor) adverse events upon the intravenous administration of SPION. A clinical study assessing the toxicity of ferumcarbotran reported adverse effects such as irritation at the site of injection, pain and headache, which were all only observed in a small subset of individuals [134]. Studies

investigating the toxicity profile of ferumoxytol and ferumoxtran reported less than 1% of serious side effects (including anaphylatic shock, chest pain, dyspnea and hypotension) and 10-20% of moderate adverse events (such as back pain, headache and urticaria) [135, 136]. The administration rate of SPION impacts the occurrence of side effects: they are observed more often when SPION are injected in bolus and they can be reduced when extending the infusion time. Overall, SPION with established coatings such as dextran are generally regarded a safe, while more exotic coatings such as PEI are typically handled with much more caution.

## 3 Diagnostic application of iron oxide nanoparticles

SPION have been extensively used for diagnostic purposes, for visualizing tumors and metastases in liver, spleen and lymph nodes [137, 138], for angiography as a blood pool agent [139] and for visualizing inflammatory lesions like atherosclerotic plaques [140]. Due to their superparamagnetic behavior, SPION shorten the relaxation time of surrounding protons. On the basis of this, they can be employed as contrast media in MRI. MR contrast agents can be divided into two major types: positive T1-weighted and negative T2/ T2*-weighted. The first class mainly shortens the T1 and at the same time provides moderate effect on the T2, generating an overall bright image. Conversely, negative contrast agents shorten T2 and lead to a dark image. Negative contrast agents show high $r_2/r_1$ ratios of at least 10. SPION mainly show a shortening effect on T2/ T2* relaxation which consequently shows a decreased signal intensity on T2/ T2*-weighted images. The use of iron oxide particles in T1-weighted imaging is limited, due to the large $r_2/r_1$ ratio. If the core size of SPION is smaller than 4 nm, a shortening of T1 relaxation times can be visualized via T1-weighted MR imaging. SPION with a core size smaller than 4 nm are known as ultra-small superparamagnetic iron oxide (USPIO) nanoparticles. An advantage over Gd-based T1 contrast agents, T1 contrast agents based on USPIO nanoparticles provide low long-term toxicity. For the formation of a suitable iron oxide based on T1 contrast agents, the size of the crystal core must be suitably designed for T1 shortening, while the effect on T2 should only be marginal. In addition, the organic shell surrounding the core needs to be stable under physiological conditions and it needs to prevent the aggregation of individual nanoparticles, as this would result in an undesired T2 contrast enhancement [141, 142]. Based on these principles, multiple iron oxide nanoparticle formulations have been employed for disease diagnosis and staging. Below, selected examples are described for the most prevalent applications.

### 3.1 Liver imaging

Like almost all other nanoparticles, intravenously administered SPION are eventually cleared by macrophages in liver, spleen, lymph nodes and bone marrow, the also called mononuclear phagocytic system (MPS) [143]. Due to their high liver uptake, iron oxide nanoparticles have been employed relatively extensively for visualizing primary lesions in the liver, e.g. in case of hepatocellular carcinoma (HCC) (Figure 3 A, B) as well as liver metastases (Figure 3 C, D) [144, 145]. Compared to healthy liver tissue, tumor lesions are characterized by lower SPION macrophage uptake as compared to healthy liver parenchyma. This reduced SPION uptake can be explained by the lower number of macrophages present

in neoplastic lesions as compared to healthy liver tissue. Similar pathophysiological phenomena are also observed in other liver diseases, such as fibrosis or cirrhosis.

Especially SPION with a hydrodynamic diameter in the range of 50-150 nm show fast accumulation in the MPS, explaining why especially these iron oxide nanoparticles have been used for liver imaging purposes [146]. Available on the market and under clinical investigation have been ferucarbotran (Resovist®) and ferumoxide (Feridex® (USA), Endorem® (EU); see Table 1 [146, 147]. When compared with each other, Chen et al. found no significant difference in signal intensity in livers on T2-weighted images for both compounds. In contrast, the determined signal intensity for ferucarbotran in the spleen was lower than for ferumoxide, due to an overall lower uptake in this organ, resulting from the smaller size and lower dose administered for ferucarbotran. In patients with liver metastasis originating from colorectal cancer, the change in contrast-to-noise was also compared for both SPION, showing a slightly less favorable contrast-to-noise ratio for ferucarbotran [148]. SPION-enhanced MRI is useful to discriminate between malignant neoplastic liver lesions (e.g. HCC or metastasis), benign neoplastic liver lesions (e.g. adenoma or hemangioma) or hyperplastic liver lesions (e.g. focal nodular hyperplasia) [149].

Apart from ferucarbotran in Japan, these agents have now been withdrawn from the market, for multiple reasons. First of all, alternatives like Primovist®, a small molecule gadolinium chelate, have become available. Gadolinium-based contrast agents show positive contrast enhancement on T1-weighted images, which is clinically generally preferred over negative T2 contrast enhancement mediated for instance by SPION [150]. Furthermore, in case of high amounts of macrophages present in the lesion, a condition often observed in well-differentiated HCC, SPION will not allow for accurate discrimination between malignant and benign liver lesions. Conversely, in such situations, Primovist® shows superiority in HCC detection, due to specific uptake by hepatocytes instead of macrophages [151]. In addition, small molecule gadolinium chelates show less body retention compared to nanoparticle-based formulations like SPION [152]. At present, ferumoxsil (Lumirem (USA), GastroMARK (EU)) is the only iron oxide nanoparticle approved by the FDA for imaging purposes. Ferumoxsil, with a hydrodynamic diameter around 300 nm, is given as an oral contrast enhancement agent for gastrointestinal imaging and examination of the bowel [153].

### 3.2 Lymph node imaging

SPION with a hydrodynamic diameter of 20-30 nm, which are referred to as ultra-small superparamagnetic iron oxide (USPIO) [154], show a prolonged circulation time and therefore are favorable for lymphography [155], for imaging inflammation [140] and for blood pool imaging [156]. When injected intravenously, USPIO circulate in the bloodstream and to some extent extravasate into tissues over time, from where they are cleared by lymphatic vessels, eventually ending up in macrophages inside lymph nodes. This results in a decrease in signal intensity in T2 and T2*-weighted MR imaging (and/or in an increase in T1-weighted imaging). Metastatic manifestation in lymph nodes compromises their function and leads to a decrease in nodal macrophage content. In addition, metastasis may lead to reduced macrophage functionality with less phagocytic activity. This results in lower USPIO

uptake and makes malignant lymph nodes appear brighter on T2/ T2*-weighted images (Figure 3 E-H).

Staging of lymph nodes is crucial in cancer classification and for choosing appropriate therapeutic regimens. Gaining knowledge on metastatic colonization of lymph nodes and on the number of affected lymph nodes helps to predict patient survival time. Lymph node staging is often performed by sentinel lymph node imaging or surgical dissection followed by histological evaluation of a few local lymph nodes draining the site of the primary tumor. Surgical dissection is invasive and not unoften associated with complications. It is applied solely to a certain area around the primary tumor and may thus lead to an underestimation of lymph node metastases manifestation by missing distant ones, mostly in the pararectal and internal iliac area. Moreover, very small lymph nodes are typically not detectable [157]. Non-invasive means for lymph node status evaluation include ultrasound (US), computed tomography (CT) and non-contrast-enhanced MRI. These techniques are clinically extensively used to stage lymph nodes according to changes in size and morphology, but they have drawbacks in terms of accuracy, specificity and sensitivity in comparison to USPIO-enhanced MR imaging [155].

Ferumoxtran (Combidex® (USA), Sinerem® (EU)) and ferumoxytol (Feraheme® (USA), Rienso® (EU)) have been in clinical trials for lymph node imaging to examine metastatic colonization [158, 159]. Recently, ferumoxtran has been re-evaluated for contrast-enhanced MRI for lymph node staging in The Netherlands, especially in the context of prostate cancer [157]. Significantly higher sensitivity for lymph node characterization in patients with prostate cancer, in which metastases detection with positron emission tomography (PET) is problematic, could be achieved by using ferumoxtran compared to non-contrast-enhanced MR imaging [160, 161]. Standard non-invasive lymph node staging according to size has limitations, such as low detection rate for very small metastases and false positive evaluation of swollen inflamed lymph nodes as metastases. By using USPIO and contrast-enhanced MRI, micro-metastatic lymph nodes can be distinguished much more efficiently from healthy and inflammatory nodes [161]. Even though ferumoxtran-enhanced MR lymphography showed high sensitivity in detection of lymph node metastases, it has not yet been implemented into clinical practice. In a multicenter clinical trial, the clinical effectiveness of contrast-enhanced MR lymphography was evaluated, producing mixed results, arguably originating from differences in the experience and expertise of the radiologists involved [162]. Ongoing research will learn whether a solid case can be made for using iron oxide nanoparticles for prostate cancer metastasis detection. In case of positive results, USPIO-based contrast-enhanced MRI may also become valuable for disease staging and therapy selection also for other cancer types in which lymph node colonization takes place, such as breast, head and neck, esophageal and pelvic cancer [158, 163–167].

### 3.3 Imaging inflammation

Macrophage infiltration can be used as a biomarker in several pathological conditions. It can for instance provide information on the stage and progression of cardiovascular disorders, such as atherosclerosis [169, 170]. To visualize and stage such inflammatory lesions, macrophages can be targeted with iron oxide nanoparticles and visualized with MRI. Several

groups have shown an increase in USPIO/ SPION uptake in vulnerable or ruptured atherosclerotic plaques in rabbits [171] and humans [172, 173] (Figure 4 A). A ruptured atherosclerotic plaque can lead to obstruction of arteries and induce a myocardial infarction, stroke or renal artery stenosis; therefore such events have to be accurately and carefully monitored [174].

In the diagnosis and staging of multiple sclerosis (MS), MRI has been used relatively extensively to evaluate the integrity of the blood-brain barrier (BBB) and to localize inflammatory lesions in the brain. In this context, a key advantage of using iron oxide nanoparticles over gadolinium-based contrast agents is the visualization of monocyte/ macrophage infiltration by the former, which correlates with ongoing demyelination and is a hallmark of disease progression in MS [175–177]. Gadolinium-based agents represent relatively non-specific and indirect imaging information on inflammation, visualizing an increase in BBB-permeability. In addition to this, USPIO nanoparticles are taken up by macrophages in the CNS and thus also provide information on macrophage content and colonization. Thus, the use of USPIO in combination with gadolinium chelates in patients with MS enables detection of additional active lesions compared to gadolinium alone (Figure 4 B). By combining both agents, higher precision in lesion detection has been achieved, which improves the identification of patients with active MS. It has been shown that lesions which appear on both gadolinium- and USPIO-enhanced images are larger and more aggressive in terms of tissue damage than lesions which only show enhancement of one of the two agents. In the future, this dual imaging agent MRI strategy may find its way into clinical application as a marker for MS disease activity [175].

Ferumoxtran-based USPIO have also been used in imaging insulitis, an autoimmune disease accompanied by leukocyte infiltration and inflammatory tissue damage of pancreatic islet cells. These islets contain insulin-producing β-cells which after damage lead to type 1 diabetes mellitus (T1D) in humans. Therefore, monitoring insulitis by imaging inflammation in the pancreas is a way for early detection of T1D. Patients suffering from insulitis showed a typical alteration in their pancreatic microvasculature due to inflammation, recognized as enhanced vascular leakiness. Circulating USPIO extravasate into the inflamed tissue and are taken up by macrophages, which leads to USPIO enrichment detectable with MRI (Figure 4C). This allows for early discrimination between diabetic and healthy individuals [178].

### 3.4 Vascular imaging

Magnetic resonance angiography is an MRI-based modality for visualizing the vasculature, especially arteries. It enables the diagnosis of vascular diseases, detecting abnormalities such as stenosis or occlusion. Compared to non-enhanced MR angiography, contrast-enhanced MR angiography has several advantages, including higher reproducibility and blood flow independency [156]. Very small superparamagnetic iron oxide particles (VSOP), with a hydrodynamic diameter around 7 nm and a short blood half-life, have been used for T1-weigthed contrast-enhanced MR angiography. Their performance was evaluated in preclinical [179] and clinical studies [180]. Even though the formulation was well-tolerated and showed favorable pharmacokinetic properties for vascular imaging, it was not further investigated in clinical trials. Small-molecule gadolinium chelates, such as gadofosveset

trisodium (Ablavar® formerly Vasovist®) tend to be preferred for this purpose. Upon injection, gadofosveset trisodium binds reversibly to human serum albumin, promoting intravascular retention and making it useful for contrast-enhanced MR angiography [181].

Due to their ability to circulate in the vascular compartment for several hours upon intravenous injection, SPION and USPIO formulation can be used as blood pool agents for the detection of endoleaks, as well as for the quantification of the relative blood volume in e.g. the brain. In comparison to small molecules, such as gadolinium chelates, they show less and less rapid extravasation into the extracellular space, resulting in higher concentrations and higher signal intensities in the vasculature. In an exemplary clinical study, Ersoy and colleagues employed ferumoxytol for the detection of aortic endoleaks after stent-graft placement [182]. They showed that iron oxide nanoparticle-enhanced MRA is superior to CT angiography for the detection of endoleaks. An added advantage using MRA instead of CT is that patients are not exposed to ionizing radiation, which is beneficial to perform longitudinal monitoring [183]. Besides ferumoxytol, also ferumoxtran and feruglose (Clariscan) have been evaluated in clinical trials for vascular imaging. Feruglose was employed for coronary angiography, contributing to the detection of coronary artery stenosis and of coronary artery bypass performance [184]. Together with thin slab 3D breath hold scans, feruglose has been proven to be suitable for the visualization of proximal coronary arteries [185]. Additionally, feruglose has been evaluated in clinical trials for contrast-enhanced MR venography, in patients with deep vein thrombosis. In this setup, it did not show superiority compared to CT-based radiographic venography [186].

Ever more evidence is accumulating that gadolinium-based contrast enhancement agents induce nephrogenic systemic fibrosis (NSF) in patients with underlying kidney disease. As a consequence, gadolinium-based contrast agents are contraindicated in patients with impaired renal function [187]. Especially for these patients, alternative MRI contrast agents like SPION may be useful. As an example, patients with kidney failure typically rely on hemodialysis for clearing their blood. This is done via an arteriovenous fistula. To assess the integrity of the fistula, ferumoxytol-enhanced MRA has been successfully employed and has shown superior image quality as compared to non-enhanced time-of-flight (TOF) MRA [188]. Within the same category of diseases, renal graft functionality after kidney transplantation is commonly evaluated by non-enhanced ultrasound. This, however, may give an incomplete picture and alternatives as contrast-enhanced MRA are considered to be useful to help resolve inconclusive results. In line with this, and with the abovementioned notion that gadolinium-based agents are contra-indicated in patients with compromised kidney function, ferumoxytol has been evaluated for imaging the renal vasculature in patients upon kidney transplantation, to determine potential renal artery stenosis and assess the overall functionality of the transplant. In this context, a study conducted by Corwin et al. investigated two different modes of ferumoxytol-enhanced MRA, and showed a clear improvement in vessel delineation for steady-state MRA compared to first-pass MRA in patients with kidney transplants [189].

Contrast-enhanced MRI is employed for brain tumor visualization and for assessing the integrity of the BBB. In general, ferumoxytol did not show superiority over gadolinium-based agents for detecting brain cancer lesions with contrast-enhanced MRI [190]. As

already mentioned, the advantage of SPION and USPIO over small molecule gadolinium chelates is their lower extravasation rate into the extravascular extracellular space. This allows a more precise determination of the relative cerebral blood volume (rCBV) and helps improving the visualization and quantification of tumor vascularization, which is an indication for brain tumor viability and progression. The standard treatment for glioblastoma multiforme (GBM) is a combination of external beam radiotherapy with temozolomide-based chemotherapy. For evaluation of treatment success (and/or monitoring of tumor progression), contrast-enhanced MRI is extensively employed. To be able to discriminate between real tumor progression and pseudoprogression (i.e. a treatment-induced inflammation which comes along with integrity loss of the BBB), the relative cerebral blood volume (rCBV) is determined after chemoradiotherapy. Low-molecular-weight gadolinium-based contrast agents show fast extravasation and thereby compromise the intravascular localization of contrast agent, which results inaccurate assessment of tumor rCBV. In contrast, ferumoxytol does not extravasate into the surrounding tissue and hence allows more reliable rCBV measurements depicting treatment success of GBM more precisely [191] (Figure 5A). In addition to this, there are increasing safety concerns related to the long-term retention of gadolinium in the brain [192]. This provides an additional rationale for the use of SPION and USPIO formulations.

In the last decade, magnetic particle imaging (MPI) has emerged as a novel and promising imaging technique. Magnetic particle imaging provides 3D information on the distribution of iron oxide nanoparticles, and has several advantages over MRI. These include the absence of potentially disturbing background signals, high temporal and spatial resolution with good quantification features, high sensitivity and fast imaging acquisition [193]. A key disadvantage as compared to MRI is that MPI does not provide anatomical information. To overcome this shortcoming, hybrid imaging approaches such as MPI/MRI and MPI/CT have been established. In vivo studies have been conducted by Kaul et al. in which measurements with preclinical 7 T MRI have been performed before and after MPI scans, to obtain the first co-registered MRI-MPI images. They successfully established the workflow and during and shortly after injection of ferucarbotran, they visualized SPION in the inferior vena cava and the heart of mice via MRI-MPI co-registration (Figure 5B). These first proof-of-principle experiments in animal models exemplify the suitability of iron oxide nanoparticle-enhanced MRI-MPI for vascular imaging [194].

MPI with iron oxide nanoparticles holds promise for cardiology applications, enabling real-time imaging without background noise. MPI is suitable for imaging vascular and cardiac perfusion as well as intervention monitoring in cardiac procedures [195, 196]. For instance, the visualization of a beating mouse heart in real-time for evaluation of cardiac functionality has been achieved with MPI with very high temporal and spatial resolution (Figure 5C). Furthermore, MPI has been shown to be able to visualize SPION-labeled catheters, providing good temporal (upon balloon filling) and spatial resolution upon the incorporation of ferucarbotran [197]. So far, MPI is not implemented in clinical routine. It may eventually find application in tracing (stem) cells, image-guided therapy and/or in combination with magnetic fluid hyperthermia (MFH) [197–200].

### 3.5 Magnetic activated cell sorting

SPION are not just employed for imaging-based diagnostic protocols. Because of their magnetic behavior, they can also be used for magnetic activated cell sorting (MACS), a standard separation method for isolating certain cell populations from biological suspensions. In MACS, magnetic nanoparticles are conjugated to antibodies which bind to specific antigens expressed on the membranes of target cells. Via this means, cells in suspension like blood samples can be specifically targeted, and upon applying a low magnetic field gradient, the target cell population can be separated from all other cells, i.e. the unbound fraction. MACS is extensively used in preclinical and clinical cancer research, as well as for sorting white blood cell populations and stem cells [201]. As such, it is an important SPION-enabled tool in biomedical research.

An important and clinically highly relevant example highlighting the relevance of MACS in clinical diagnostic protocols is its use for capturing and analyzing circulating tumor cells (CTC). Sorting and detecting CTC is becoming increasingly relevant in cancer staging, therapy selection and treatment monitoring. Moreover, it has been shown that CTC can already be found in peripheral blood during early stages of malignancy, when no primary tumor can be detected using conventional methodologies [202]. In principle, several standard techniques are available for cell isolation and sorting and counting. Most of them, however, like filtration, sedimentation and centrifugation, are purely based on physical properties such as cell size. In situations where physical differences are not really noticeable – such as analysis of CTC – more specific separation methods are needed, making MACS (pre-) clinically very useful. Another key advantage of MACS is its high sensitivity. As an example, less than 50 CTC can be accurately detected in up to 10 billion total blood cells [203]. MACS is increasingly being proven to be an effective and robust diagnostic tool for detecting, sorting and analyzing specific cell populations with high sensitivity. As such, it may become useful for early cancer diagnosis, for staging and for treatment monitoring.

### 3.6 Magnetic nanoparticle-based biosensors

Magnetic nanoparticles can also be used as sensors in devices, for sensitively measuring molecular interactions. In this context, Weissleder and colleagues developed a chip-based diagnostic magnetic resonance (DMR) system for the detection of nucleic acids [204], proteins and pathogens in unpurified biological samples [205, 206]. The magnetic nanoparticles are conjugated to ligands such as antibodies or oligonucleotides, which upon binding to the target side begin to cluster. The assembly of the magnetic nanoparticles induces a decrease in T2 of the surrounding water molecules which is detectable by nuclear magnetic resonance (NMR) or by MRI [207]. This DMR system has been tested for the detection of cancer biomarkers in serum samples [205]. A study conducted by Wildgruber et al. investigated small volumes of human blood for alterations in monocyte subtype populations, which can serve as a biomarker for cardiovascular diseases or inflammatory processes. The chip-based DMR system was used for the quantification of shifts in monocyte subtype distribution in inflammatory atherosclerosis in humans, thereby potentially contributing to the identification of patients at risk for atherosclerotic plaque rupture [208]. Advantages of these particular chip-based devices and detection methods include the straightforward and easily scalable production of the device, the relatively low

costs of the diagnostic assessment, the high sensitivity, and the possibility to perform measurements in very small sample volumes, together rendering the DMR system suitable for future clinical application [205].

## 4 Therapeutic application of iron oxide nanoparticles

### 4.1 Anemia

Besides for diagnostic purposes, iron oxide nanoparticles have also been used for therapeutic application, for instance to supplement iron in individuals with iron deficiency. Ferumoxytol is clinically used to treat anemia in patients with chronic kidney disease (CKD). This SPION formulation was initially developed for sentinel lymph node and atherosclerotic plaque imaging, but did not manage to outperform alternative diagnostic probes and protocols. In 2009, it received FDA approval for the treatment of iron deficiency in CKD patients [209]. In this group of diseases, the renal function of the patient is impaired and the production of erythropoietin, a hormone that promotes the synthesis of erythrocytes, can be dramatically decreased, leading to anemia. By administering ferumoxytol intravenously (IV), the iron levels in the blood and in macrophages in the liver, the spleen and elsewhere become elevated, and over time the total pool of iron in the body is normalized. This in turn promotes erythrocyte production, relieves anemia and contributes to an improved well-being of the patient.

### 4.2 Modulating macrophage polarization

Iron oxide nanoparticles have recently been shown to possess pharmacological properties, altering the polarization of the macrophages in which they accumulate. Macrophages are historically divided into two subtypes, based on their functionality: M1 macrophages which display pro-inflammatory and anti-tumor activity; and M2 macrophages which display an anti-inflammatory and pro-tumor phenotype. We nowadays know that these two classifications do not really reflect realistic in vivo conditions, and that they are the extreme opposing ends of a whole spectrum of possible macrophage polarization states. Macrophages, as part of the innate immune system, play an important role in cancer progression. It has been shown that cancer cells are able to modulate the immune system, and by secreting certain chemo- and cytokines, like the C-C motif chemokine ligand 2 (CCL2), they are able to recruit monocytes. In the tumor microenvironment, the attracted monocytes are exposed to cytokines like the macrophage colony-stimulating factor (M-CSF), which push macrophage differentiation towards a tumor growth supporting phenotype. These so-called tumor-associated macrophages (TAM) produce and release e.g. interleukin-1 (IL-1) and vascular endothelial growth factor (VEGF), which support tumor growth and progression and which induce angiogenesis [210]. Recently, after exposing TAM to iron oxide nanoparticles, a shift in polarization towards a more M1-like phenotype and an increase in the production of reactive oxygen species (ROS) could be observed. These features can either be used directly against cancer cells (e.g. via ROS; Figure 6A) or indirectly, via inducing changes in the tumor microenvironment (TME), such as normalization of the vasculature [211].




Europe PMC Funders Author Manuscripts

Initial evidence linking iron metabolism to macrophage polarization was provided by Sindrilaru and colleagues [212]. They investigated human chronic venous leg ulcers (CVU) by using a mouse model for mimicking the pathology of the disease. They administered iron dextran intravenously to induce iron overload in mice with acute wounds, and monitored wound healing and macrophage polarization. They observed impaired wound healing compared to the non-iron-treated control group. To explain their findings, they correlated the delay in wound healing with the increase in M1-like pro-inflammatory macrophages induced by the administration of iron dextran. The macrophage phenotype was persistent pro-inflammatory and intermediate anti-inflammatory with high expression levels of TNFα, interleukin-12 (IL-12), chemokine receptor type 2 (CCR2) and lymphocyte antigen 6 complex (Ly6C), and medium expression levels of Dectin-1, interleukin-4 receptor alpha (IL-4Rα) and CD204. This supports the hypothesis, that iron dextran affects macrophage polarization by inducing a phenotypical shift towards an inflammatory state. In vitro studies conducted by Laskar et al. support these findings, showing a similar behavior when human macrophages were treated with SPION. During their investigations, they pre-polarized THP-1 monocytes towards an M2-like activation state and exposed them to SPION to see if and how the treatment influences macrophage activity. As in the above study, they observed a shift in phenotype towards M1, which comes along with an increased expression of CD86, TNFα and intracellular ferritin [213]. These studies exemplify the immunomodulatory properties of iron oxide nanoparticles in vitro and in vivo, and provide a basis for further investigation of their tumor growth inhibitory effects via modulating macrophages.

In the last 5 years, many studies have shown that SPION can influence macrophage polarization. A key paper in this regard has been published by Zanganeh and colleagues, showing that the tumor growth inhibition caused by ferumoxytol is mediated by a shift in macrophage polarization towards a M1-like phenotype and to a concomitant increase in ROS production [214] (see Figure 6 B-C). These results have been confirmed by Costa de Silva et al., who investigated the effect of red blood cells (RBC) and cross-linked iron oxide nanoparticles on macrophage polarization and tumor growth in a small cell lung cancer model. Vinchi and colleagues showed that the iron species used and the route of uptake is not crucial for the outcome of macrophage polarization, as evidenced by the fact that also even heme and simple iron chelates can induce a phenotypical shift in macrophages [215]. Besides their direct effects on macrophage polarization and tumor growth, the use of SPION is also interesting in a (neo-) adjuvant setting, e.g. in combination with immunotherapy. In this context, future studies will undoubtedly explore if, when and how iron oxide nanoparticles can be employed to prime the tumor immune microenvironment (TME), for better outcome of e.g. checkpoint blockade treatments.

### 4.3 Magnetic fluid hyperthermia

In magnetic fluid hyperthermia (MFH), iron oxide nanoparticles are exposed to an alternating external magnetic field that triggers motion of the particles and local heating. This hyperthermic effect can lead to tissue damage in the nanoparticles' surrounding area and has been applied in tumor therapy [216]. The main effect is based on the increase of the temperature above 42 °C and to the resulting denaturation of proteins, together leading to cell death [217] (Figure 7A). The temperature increase induced by magnetic fluid

hyperthermia resulting from intravenously administered SPION is generally not sufficiently high to be employed curatively in cancer therapy, due to a too low accumulation of the nanoparticles locally at the tumor site. To maximize MFH performance, in the clinic, they are therefore typically injected directly into the tumor via a catheter (Figure 7 B-D).

One of the formulations now available on the market for MFH is a SPION formulation referred to as Nanotherm®. It has a hydrodynamic diameter of 15 nm and an amino-silane coating. So far, it has been tested as an anticancer treatment for glioblastoma[220], prostate [221] and pancreatic cancer in preclinical settings, and for glioblastoma [219] and prostate cancer [222] in clinical trials. A clinical phase II single-arm study was conducted by Maier-Hauff et al, in which MFH was combined with radiotherapy in patients with recurrent glioblastoma. As reference, they chose historical controls from former studies where the patients obtained chemotherapy (temozolomide) following glioblastoma recurrence [223, 224]. An increase of median survival of 13.4 months for patients treated with a combination of MFH and radiotherapy after glioblastoma recurrence was obtained (Figure 7E). As compared to the abovementioned historical control group, where the median survival after recurrence was 6.2 months, this increase is substantial.

Disadvantages of MFH modality include the necessity of removing all metals in the head area, including tooth fillings. In addition, MRI for evaluation of tumor progression cannot be properly performed after MFH, because of the artifacts caused by the very high amounts of SPION that accumulate in the lesion [219]. Therefore, other imaging techniques, like CT, positron emission tomography (PET) or single-photon emission computed tomography (SPECT), have to be employed to faithfully monitor therapy response and tumor growth.

### 4.4 Magnetic drug targeting

Magnetic drug targeting has been extensively explored to enhance the accumulation of intravenously injected SPION at pathological sites. In magnetic drug targeting, SPION are guided by a strong, external magnetic field gradient to a specific target side, e.g. a tumor, where an alternating magnetic field can then induce hyperthermia or inducible drug release [68].

Magnetic drug targeting has produced mixed results, sometimes with substantial increase in the amount of iron oxide nanoparticles accumulating in tumors upon exposure to a magnetic field, and sometimes with minimal effects when administering SPION intravenously. The latter case might be explainable by the minimal magnetic force generated from small magnetic cores of commonly used SPION. In an elegant study, Al-Jamal and colleagues mathematically modeled and systematically studied magnetic drug targeting for the evaluation of targeting efficacy in terms of SPION loading. They developed PEGylated oil-cored magnetic nanocapsules (NC), all with a hydrodynamic diameter around 200 nm, loaded with increasing amounts of SPION. The in vivo results showed that magnetic targeting in CT26 tumor bearing mice was directly proportional to SPION loading and magnetic field strength. Compared to other SPION, with smaller magnetic cores, they showed improved magnetic targeting properties, even though the nanocapsules may not be in the ideal size range for tumor accumulation mediated by the enhanced permeability and retention effect (EPR; the pathophysiological phenomenon leading to enhanced nanoparticle

accumulation in neoplastic and inflammatory lesions via leaky vasculature and lacking lymphatic drainage). Furthermore, they used their experimentally obtained data on the magnetic forces acting on nanocapsules in vivo to develop a mathematical model, and they extrapolated this to humans. They concluded that their magnetic drug targeting approach would be feasible in human, if particles of the right size and the right SPION content can be employed. This is an important first step to overcome the gap between preclinical and clinical experiences in the area of magnetic drug targeting [225].

Magnetic drug targeting is typically employed with the aim of enhancing the accumulation and the efficacy of iron oxide nanoparticles loaded with chemotherapeutic drugs. Besides chemotherapeutics, also more advanced agents such as DNA, siRNA and radionuclides [226–228] have been combined with SPION and magnetic drug targeting [229]. Specifically for nucleic acid delivery, a technique termed magnetofection has been established [230, 231]. From a translational point of view, only one magnetically targeted nanocarrier (which was loaded with doxorubicin; MTC-DOX) has been evaluated in patients, but it did not produce convincing results, leading to termination of clinical development in phase II/III [232, 233]. A major limitation of this method is the precise application of the magnetic field when targets deep within the body need to be addressed. Furthermore, magnetic drug targeting needs very strong magnetic fields for successful application in humans, which increases the cost of the hardware setup, and which makes it less attractive for clinical implementation [199].

## 5 Theranostic applications of iron oxide nanoparticles

The term theranostics refers to the combination of diagnosis and therapy. From a clinical and translational point of view, it relates to an intimate combination of diagnostic and therapeutic interventions, as e.g. for staging and treatment of patients with thyroid cancer with radioactive iodine, or to perform patient selection and treatment of somatostatin receptor-expressing neuroendocrine neoplasias with DOTATOC/TATE-based theranostic pairs (e.g. gallium and yttrium). In the nanomedicine field, the term theranostics is often used when imaging agents and drug molecules are co-loaded in one nanoparticle. Iron oxide nanoparticles are intrinsically very suitable for theranostic purposes, because of their ability to be visualized by MRI or MPI, while their shell can be physically or chemically loaded with therapeutic agents. Iron oxide nanoparticles can also be easily integrated in microbubbles and in macroscale materials for tissue engineering, contributing to the range of theranostic applications for which they can be used.

### 5.1 Companion diagnostics

Nanoparticles accumulate in tumors (and also at sites of inflammation) via the enhanced permeability and retention (EPR) effect. In the last couple of years, it has become increasingly recognized that the EPR effect is a highly heterogeneous phenomenon, especially in cancer. Variability if high between different tumor types, between different patients with the same tumor type, and between different tumors and metastasis in the same patient. This variability is considered to be one of the key reasons for the heterogeneous

outcomes of clinical trials in which chemotherapy-loaded nanomedicine formulations have been tested in patients.

Based on the co-localization of nanoparticles applied for imaging (such as SPION) and therapeutic nanoparticles, iron oxide-based companion diagnostics can be applied to visualize and quantify EPR effect in individual patients, and to thereby predict therapy responses. This personalized approach may help to discriminate between responders and non-responders of nanodrug therapy in a straightforward, cost-efficient way [234]. In this context, Miller et al. studied the intratumoral distribution of ferumoxytol and PLGA-PEG nanoparticles, both fluorescently labeled, in subcutaneous HT1080 human fibrosarcoma xenografts in nude mice and showed co-localization of both particles. They used the same tumor model to investigate the accumulation rate of ferumoxytol with MRI. Based on that, they were able to predict the treatment efficacy of paclitaxel-loaded PGLA-PEG nanoparticles [235] (Figure 8 A-B). This study exemplifies how imaging may be used in patient selection for nanoparticle treatment.

Recently, Ramanathan et al. tested this concept in the clinic. They evaluated the accumulation of ferumoxytol with MRI in patients with metastatic solid tumors, and they correlated iron oxide nanoparticle accumulation with therapy response induced by irinotecan-loaded liposomes (Onivyde®). They first showed a highly heterogeneous uptake of ferumoxytol in different cancer lesions within patients, as well as across the whole patient population (Figure 8C). Next, they monitored individual lesion response upon Onivyde® treatment in terms of tumor size reduction via CT scans, and they then correlated treatment response with ferumoxytol accumulation for each of the individual lesions and patients. They found a statistically significant correlation between changes in lesion size and lesion uptake of ferumoxytol (Figure 8D). This suggests that ferumoxtol uptake may serve as a suitable and clinically very useful imaging biomarker for monitoring the EPR effect and predicting nanotherapy treatment responses [236].

### 5.2 Theranostic iron oxide-based nanoformulations

Instead of using a companion diagnostic nanoparticle to monitor target site accumulation and predict therapy response, imaging capabilities and therapeutic properties can also be combined in a theranostic nanoparticle. In this context, the shell of iron oxide nanoparticles can for instance be modified with pharmacologically active compounds. This can either be done via chemical conjugation and a cleavable linker, or via physical intermolecular interactions, such as π-π stacking. SPION have been loaded with many different therapeutics drugs. Especially anticancer agents have been employed, ranging from standard low molecular weight chemotherapeutics, such as doxorubicin, to more advanced therapeutic compounds, such as siRNA [237, 238].

In such setups, iron oxide nanoparticle-association prevents fast excretion or degradation, and it thereby increases the circulation time and the target site accumulation of the drugs. Medarova and colleagues conjugated siRNA to SPION, additionally modified them with a membrane translocation peptide and with a near-infrared dye, for multimodal image-guided siRNA delivery. After evaluation of tumor accumulation with MRI and near-infrared in vivo optical imaging, they evaluated the silencing efficacy of this theranostic nanomaterial in 9L

or LS174T tumor-bearing mice. They achieved substantial silencing (of both GFP and survivin) in tumors, which was comparable or superior to previous published studies. This study thereby provided pioneering proof-of-concept for a SPION-based theranostic nanoplatform for siRNA delivery [239].

To enhance the accumulation and/or the uptake of nanomedicine formulations, various active targeting strategies have been explored. In such setups, targeting ligands like antibodies, peptides or aptamers are attached to the shell of iron oxide nanoparticles[240–242]. One has to keep in mind in this regard that active targeting strategies do not necessarily result in increasing the target site accumulation of nanoparticle formulations. More rapid recognition of ligand-modified particles by phagocytic cells in liver, spleen and other organs of the MPS often results in reduced circulation times, and thus in less strong tumor accumulation via the EPR effect. In addition to this, nanoparticles often do not penetrate deeply into the extravascular space in target tissues. This is especially problematic in highly stromal tumors. As a result of this, depending on the therapeutic direction chosen, intravascular targets which are highly expressed on the surface of endothelial cells may be preferred for active targeting. Easily accessible targets for theranostic SPION for instance are integrins, especially the $\alpha_v\beta_3$-integrin, which is overexpressed on angiogenic endothelium. In a study conducted by Schleich et al., a head-to-head comparison of different targeting strategies for SPION has been performed [243]. The study investigated the accumulation rate and treatment success of standard passively targeted paclitaxel (PTX) -loaded SPION, of actively vessel-targeted RGD-peptide-modified PTX-SPION, and of the combination of both with magnetic targeting. The study was performed in mice bearing CT26 colon carcinomas. In this setup, the longest overall survival was achieved upon the combination of active and magnetic targeting [243]. These findings are consistent with the expected outcome, but they also need to interpreted with care. In terms of both active targeting and magnetic targeting, which may both not be easily reproducible and easily translatable to the clinic.

The real-life situation in cancer patients is much more diverse than that in animal models. Even though a variety of promising preclinical data exists and has shown somewhat promising results, none of the designed and evaluated actively targeted and magnetic SPION have thus far been translated to the clinic. However, the importance of personalized therapy and theranostics is rising, and scientists and companies have realized that patient stratification has to be integrated in translational nanomedicine research, to maximize the chances of successful therapy outcome. Theranostic nanoparticles provide a useful tool to gain knowledge about biodistribution and target site accumulation, and thus help to preselect patients and predict therapy responses [244].

### 5.3 Theranostic iron oxide nanoparticle-loaded microbubbles

Microbubbles (MB) are gas- or air-filled microvesicles surrounded by a lipidic, polymeric or protein-based shell. MB are extensively used for diverse biomedical applications. Besides their routine use as intravascular contrast agents for contrast-enhanced ultrasound (US) imaging, they are also used for direct and indirect drug delivery purposes [245, 246]. In case of indirect drug delivery, the use of US and MB increases the permeability of vascular endothelium and cellular membranes, through a process called sonoporation, thereby

promoting the uptake of therapeutic compounds at target sites and in target cells [247, 248]. Examples of MB formulations that have or had been clinically approved are Lumason® or SonoVue® (sulphur hexafluoride as core gas; phospholipid shell; mean diameter of 2-8 μm), Luminity® or Definity® (perfluoropropane as core gas; phospholipid shell; mean diameter of 1.1-2.5 μm), Optison™ (perfluoropropane as core gas; human albumin shell; mean diameter of 3-4.5 μm), Sonazoid™ (perfluorobutane as core gas; phospholipid shell; mean diameter of 2.6 μm), Albunex® (air-filled; human serum albumin shell; mean diameter of 4 μm), and Levovist® (air-filled; galactose (99.9%) and palmitic acid (0.1%) shell; mean diameter of 2-5 μm) [249–253].

The shell of MB can be loaded with iron oxide nanoparticles, for image-guided drug delivery purposes. This seems especially useful when performing sonoporation of the blood-brain barrier (BBB). Disorders of the central nervous system, such as Alzheimer and Parkinson's diseases, as well as brain tumors, require systemic treatment with drugs that are able to cross the BBB. Theranostic MB with iron oxide nanoparticles within their shell have been employed to enable efficient and safe drug delivery across the BBB, via monitoring of BBB permeation. In this setup, upon exposure to US pulses, USPIO-loaded MB are destroyed promoting BBB opening. During this process, the iron oxide nanoparticles are released from the MB shell and they extravasate across the permeabilized BBB, accumulating in extravascular brain tissue and providing MRI information on the kinetics and the extent of BBB opening (Figure 9A). BBB opening was verified using i.v. administered fluorophore-labeled dextran, which only accumulates in the brain in case of sonoporation. A good correlation between dextran accumulation in the brain and iron oxide nanoparticle-based MR imaging information was observed, exemplifying that such theranostic MB hold potential for image-guided drug delivery to the brain. Especially important in this context is the use of imaging guidance to lower toxicity. Since the BBB is of vital importance for proper brain function, opening of the BBB should only be done very carefully, upon minimal ultrasound exposure, and for a period of time as short as possible, allowing for efficient drug delivery, but not causing side effects. To achieve this, theranostic systems and strategies are considered to be of crucial importance. To extend this concept towards clinical translation, multiple aspects have to be further studied and refined, including e.g. MB concentration, MB size, MB composition, iron oxide nanoparticle content, and ultrasound power and frequency [247, 254, 255].

### 5.4 Theranostic iron oxide nanoparticle-containing materials in regenerative medicine

Iron oxide nanoparticles can be used for several aspects of regenerative medicine, for instance as a tracer to track cells. The application of cells for therapeutic purposes offers novel approaches to combat diseases like cancer, neurodegenerative disorders or immunological pathologies. In this context, stem cells as well as immune cells such as T cells [259] and dendritic cells [126] have been labeled with SPION to allow for noninvasive tracking via MR imaging and to monitor in vivo delivery to the site of action [260]. The labeling of such cells, as well as of progenitor cells and monocytes/macrophages can be readily achieved in vitro, by incubating them with SPION in the presence or absence of a transfection agent. Depending on the phagocytic activity of the cell type studied, transfection may be necessary to promote SPION uptake. In case of phagocytes, like macrophages, this

is not needed, but for non-phagocytic cells, like stem cells, cationic materials such as poly-L-lysine or protamine are typically employed to increase the otherwise very low SPION uptake [254].

In cancer immunotherapy, dendritic cells are explored for immune system activation to promote eradiation of tumor cells. In such setups, dendritic cell vaccines are loaded with tumor antigens, which after successful injection into lymph nodes, will display the antigens to T-cells. To ensure the successful injection and delivery of autologous dendritic cells, De Vries et al. labeled them with SPION and with $^{111}$In-oxine and, upon injection into lymph nodes, followed their biological fate in melanoma patients by MRI and scintigraphy. The delivery of the dendritic cell vaccines could be more accurately visualized and verified by MRI as compared to scintigraphy. Both methods showed similar sensitivity but misadministration (next to rather than into the lymph node) could only be detected by MRI [126]. Besides in such dendritic cell-based cancer immunotherapies [261], SPION have been also employed in other immune system activation strategies such as ex vivo T cell stimulation or thermal ablation induced immunity [262, 263].

Stem cells are under investigation for the treatment of many different pathologies, including e.g. neurodegenerative, musculoskeletal and cardiovascular diseases. To improve understanding and ensure successful treatment, monitoring the in vivo fate of implanted or injected stem cells is very valuable. SPION-labeling in combination with MRI (and recently also MPI) has been the method of choice for cell tracking [193, 255]. In an exemplary recent in vivo study, ferucarbotran-labeled neuronal progenitor cells (NPC) have been implanted in the forebrain of rats with forebrain ischemia, and investigated longitudinally with MPI [198] (Figure 9B). After injection, the cells could be sensitively and specifically detected with MPI for up to 87 days. As controls, the authors either injected only ferucarbotran into the forebrain, or they injected ferucarbotran-labeled NPC near the lateral ventricle. In case of the former, the MPI signal was not detectable for a prolonged period of time, indicating low retention of ferucarbotran itself in the brain. For the other control group, an additional signal caudal/posterior to the injection site appeared, indicating gradual clearance of the labeled cells through the ventricle. The study therefore nicely exemplifies the feasibility of long-term cell tracking with MPI. Neuronal progenitor and stem cells have been implicated in the treatment of multiple severe neurodegenerative disorders, such Parkinson's Disease, Alzheimer's Disease and Huntington's disease, and brain ischemia [256]. Also for pathologies, SPION-labeled stem cells have been explored. Several clinical studies have been performed with SPION-loaded cells, including e.g. labeled neuronal stem cells for traumatic brain injury and labeled pancreatic islet cells for diabetes [257, 258]. Thus far, however, none of these theranostic concepts for regenerative medicine are employed in clinical practice.

Besides for cell labeling, iron oxide nanoparticles can also be used to visualize scaffold materials in regenerative medicine applications. This provides the possibility to get information on and obtain control over the proper positioning of these materials, and to ensure their proper functionality over time. Furthermore, noninvasive imaging can be employed to monitor scaffold degradation. Together, this enables the visualization and quantification of multiple important processes in tissue engineering. When combining cells

with scaffolds, as is routinely done in tissue engineering applications, both components can thus be labeled via simple and straightforward means with iron oxide nanoparticles, depending on what type of information is needed to maximize therapeutic performance.

In study published by Liu et al, mesenchymal stem cells (MSC) were embedded in a collagen-based hydrogel and injected subcutaneously. Before administration, the cells were loaded with amphiphilic polyethylenimine / iron oxide nanocomposites for in vivo tracking of the biohybrid implant. The fate of the construct was monitored for up to 19 days on a clinical 3 T MRI device. If compared with the scaffold containing non-labeled cells, a clear hypointense area was visible, indicating the presence of the labeled cells in the implant (Figure 9C). After 19 days, the implanted collagen hydrogels were isolated and analyzed by H&E and Prussian blue staining. This identified numerous viable MSC with a high amount of ingested iron, responsible for the high T2 relaxivity [264]. Since MSC are capable of differentiating into a variety of other cells, including adipocytes, osteoblasts, chondrocytes, myoblasts and neuron-like cells, they are highly useful and often employed in regenerative medicine applications [264, 265].

Collagen is frequently used as a scaffold material, especially for bone tissue engineering. Mertens et al. labeled collagen scaffolds with iron oxide nanoparticles for image-guided tissue engineering. They tested different ways of USPIO incorporation into the collagen scaffold, either via chemical conjugation, or via physical means, i.e. passive incorporation during collagen crosslinking. They extensively characterized the different scaffolds and visualized them longitudinally in mice for up to 22 days. They were able to precisely localize the implants and sensitively image them by MRI (Figure 9D). In addition, they provided initial experimental evidence showing that scaffold labeling may allow for the visualization and quantification of scaffold degradation [266].

The same team of authors also prepared iron oxide nanoparticle-labeled scaffold materials for visualizing tissue-engineered vascular grafts. To this end, polyvinylidene fluoride-based textile fibers were loaded with USPIO, and they were employed as the starting material to construct a biohybrid blood vessel for vessel replacement therapy. The scaffold was initially functionalized with fibrin, fibroblasts and smooth muscle cells, after which it was bioreactor-cultivated for two weeks. Afterwards, autologous endothelial cells were introduced into the lumen of the vessel and allowed to adhere. Subsequently, the endothelialized vascular graft was cultivated in a bioreactor for another 8 days under physiological flow and pressure conditions. The graft was then implanted as an arteriovenous shunt in sheep. As shown in Figure 9E, they were able to visualize and localize the USPIO-labeled graft with high precision, which was not the case for an unlabeled control vascular graft [267]. They also showed good biocompatibility and functionality (via time-of-flight angiography) of the graft, and proper in vivo integration into surrounding tissue, with even endogenous blood vessels having formed within the graft. Such theranostic tissue engineering approaches hold significant potential, and iron oxide nanoparticles undoubtedly are among the most attractive imaging agents for implementation in theranostic tissue engineering.

Europe PMC Funders Author Manuscripts

## 6 Conclusions

Iron oxide nanoparticles possess many unique and attractive properties, explaining their extensive use in biomedical research. In this review, we summarize recent advances in the development of iron oxide nanoparticles for in vitro and in vivo biomedical applications, focusing primarily diagnosis, therapy and theranostics.

Iron oxide nanoparticles can be synthesized by multiple different techniques, which all have their own advantages and disadvantages. Co-precipitation, thermal decomposition, microemulsion and sol-gel are the most commonly employed synthetic techniques. Core size, size distribution, crystallinity, shape and saturation magnetization are key parameters that have to be controlled to tailor nanoparticle properties for biomedical applications. The surface modification of iron oxide nanoparticles, typically done with polymers, helps to improve biocompatibility, colloidal stability in complex biological environments and in vivo performance.

Iron oxide nanoparticles are extensively used for diagnostic purposes. Depending on their core size, iron oxide nanoparticles can be either used as T1-weighted or T2/T2*-weighted MR contrast agents. Ferucarbotran and ferumoxide have been employed for visualizing liver tumors and metastases. Ferumoxsil is approved by the FDA as an orally administered contrast agent for gastrointestinal imaging. Ferumoxtran and ferumoxytol are in clinical trials for imaging lymph node metastais, especially in prostate cancer. Ferumoxtran-based USPIO have been tested for imaging insulitis, and ferumoxytol, ferumoxtran and feruglose have been evaluated as blood pool agent for vascular imaging.

Iron oxide nanoparticles have also been used for therapeutic purposes. Ferumoxytol has received FDA approval for the treatment of anemia in CKD patients. It has also been shown to influence macrophage polarization, which may find future application in multimodal cancer therapy, for instance to prime the tumor microenvironment for better immunotherapy outcomes. Magnetic drug targeting and magnetic guidance of devices are extensively explored preclinically, and they may one day find application in a specified sub-set of pathologies. NanoTherm™ is an iron oxide nanoparticle formulation that is now available on the market for magnetic fluid hyperthermia.

Because of their nanosize and their intrinsic imaging capabilities, iron oxide nanoparticles are exquisitely suitable for theranostic applications. Several initial clinical proof-of-concept studies in this regard have already been performed. These include the use of ferumoxytol as a companion diagnostic in tumor-targeted nanotherapy settings. Numerous theranostic iron oxide-based nanoparticles have been designed and tested for drug delivery applications, especially for cancer, and oftentimes combined with magnetic drug targeting or magnetic fluid hyperthermia. Iron oxide nanoparticles in microbubbles can help to obtain valuable information on the efficacy of sonoporation, which holds potential to enhance drug delivery to tumors and to the brain. Finally, also in regenerative medicine, iron oxide nanoparticles are often employed in theranostic setups. Besides (stem) cell tracking, which has already been done in the clinic, also scaffold materials are nowadays routinely labeled with iron oxide nanoparticles. This allows for the visualization of the tissue-engineered implants

during and after implantation, for assessing their engraftment and degradation, and for longitudinally monitoring their functionality and performance.

Taking everything together, there seems to be a bright and broad future ahead for the use of iron oxide nanoparticles for biomedical applications. After several initial setbacks, in which ferucarbotran and ferumoxide were initially marketed and later on again withdrawn (because of the availability of better alternatives for the diagnostic applications in question), there are now numerous different preclinical directions that are being explored, and also more and more clinical applications that involve the use of iron oxide nanoparticles. In the future, advanced imaging techniques (such as MPI) and advanced therapeutic concepts (such as stem cell therapy and tissue engineering) will become more and more established. Since iron oxide nanoparticles play a key role in eventually making these technologies and therapies useful and successful, research and development in this area of research will definitely continue to flourish. As a result of this, it is foreseen that in the next 1-2 decades, multiple iron oxide nanoparticle-based diagnostics, drugs and devices will become routinely used in clinical practice.

## Acknowledgments

The authors gratefully acknowledge financial support by the European Research Council (ERC: Starting Grant 309495 (NeoNaNo) and Proof-of-Concept Grants 680882 (CONQUEST) and 813086 (PIcelles)), by the European Union (ERA-Net EuroNanoMedicine-III: NSC4DIPG), by the German Research Foundation (DFG: La2937/1-2, SFB/TRR57, SFB1066 and GRK2375) and by the Interdisciplinary Center for Clinical Research at RWTH Aachen University Hospital (IZKF).

## References

[1]. Figuerola A, Di Corato R, Manna L, Pellegrino T. From iron oxide nanoparticles towards advanced iron-based inorganic materials designed for biomedical applications. Pharmacol Res. 2010; 62:126–143. [PubMed: 20044004]

[2]. Mohammed L, Gomaa HG, Ragab D, Zhu J. Magnetic nanoparticles for environmental and biomedical applications: A review. Particuology. 2017; 30:1–14.

[3]. Wu W, Wu Z, Yu T, Jiang C, Kim W-S. Recent progress on magnetic iron oxide nanoparticles: synthesis, surface functional strategies and biomedical applications. Sci Technol Adv Mater. 2015; 16

[4]. Jin R, Lin B, Li D, Ai H. Superparamagnetic iron oxide nanoparticles for MR imaging and therapy: design considerations and clinical applications. Curr Opin Pharmacol. 2014; 18:18–27. [PubMed: 25173782]

[5]. Cheng F-Y, Su C-H, Yang Y-S, Yeh C-S, Tsai C-Y, Wu C-L, Wu M-T, Shieh D-B. Characterization of aqueous dispersions of Fe3O4 nanoparticles and their biomedical applications. Biomaterials. 2005; 26:729–738. [PubMed: 15350777]

[6]. Xu H, Cheng L, Wang C, Ma X, Li Y, Liu Z. Polymer encapsulated upconversion nanoparticle/iron oxide nanocomposites for multimodal imaging and magnetic targeted drug delivery. Biomaterials. 2011; 32:9364–9373. [PubMed: 21880364]

[7]. McCarthy JR, Weissleder R. Multifunctional magnetic nanoparticles for targeted imaging and therapy. Adv Drug Deliv Rev. 2008; 60:1241–1251. [PubMed: 18508157]

[8]. Lee N, Hyeon T. Designed synthesis of uniformly sized iron oxide nanoparticles for efficient magnetic resonance imaging contrast agents. Chem Soc Rev. 2012; 41:2575–2589. [PubMed: 22138852]

[9]. Khandhar AP, Ferguson RM, Arami H, Krishnan KML. Monodisperse magnetite nanoparticle tracers for in vivo magnetic particle imaging. Biomaterials. 2013; 34:3837–3845. [PubMed: 23434348]

[10]. Du Y, Lai PT, Leung CH, Pong PW. Design of superparamagnetic nanoparticles for magnetic particle imaging (MPI). Int J Mol Sci. 2013; 14:18682–18710. [PubMed: 24030719]

[11]. Ferguson RM, Khandhar AP, Kemp SJ, Arami H, Saritas EU, Croft LR, Konkle J, Goodwill PW, Halkola A, Rahmer J. Magnetic particle imaging with tailored iron oxide nanoparticle tracers. IEEE Trans Med Imaging. 2015; 34:1077–1084. [PubMed: 25438306]

[12]. Weizenecker J, Gleich B, Rahmer J, Dahnke H, Borgert J. Three-dimensional real-time in vivo magnetic particle imaging. Phys Med Biol. 2009; 54

[13]. Schleich N, Danhier F, Préat V. Iron oxide-loaded nanotheranostics: Major obstacles to in vivo studies and clinical translation. J Control Release. 2015; 198:35–54. [PubMed: 25481448]

[14]. Mahmoudi M, Sant S, Wang B, Laurent S, Sen T. Superparamagnetic iron oxide nanoparticles (SPIONs): development, surface modification and applications in chemotherapy. Adv Drug Deliv Rev. 2011; 63:24–46. [PubMed: 20685224]

[15]. Laurent S, Dutz S, Häfeli UO, Mahmoudi M. Magnetic fluid hyperthermia: focus on superparamagnetic iron oxide nanoparticles. Adv Colloid Interface Sci. 2011; 166:8–23. [PubMed: 21601820]

[16]. Hedayatnasab Z, Abnisa F, Daud WMAW. Review on magnetic nanoparticles for magnetic nanofluid hyperthermia application. Mater Des. 2017; 123:174–196.

[17]. Perigo EA, Hemery G, Sandre O, Ortega D, Garaio E, Plazaola F, Teran FJ. Fundamentals and advances in magnetic hyperthermia. Appl Phys Rev. 2015; 2

[18]. Haun JB, Yoon TJ, Lee H, Weissleder R. Magnetic nanoparticle biosensors. Wiley Interdiscip Rev Nanomed Nanobiotechnol. 2010; 2:291–304. [PubMed: 20336708]

[19]. Siddiqi KS, Rahman A ur, Husen A. Biogenic fabrication of iron/iron oxide nanoparticles and their application. Nanoscale Res Lett. 2016; 11:498. [PubMed: 27837567]

[20]. Tan SC, Yiap BC. DNA, RNA, and protein extraction: the past and the present. BioMed Res Int. 2009; 2009

[21]. Gupta AK, Naregalkar RR, Vaidya VD, Gupta M. Recent advances on surface engineering of magnetic iron oxide nanoparticles and their biomedical applications. 2007

[22]. Qiao R, Yang C, Gao M. Superparamagnetic iron oxide nanoparticles: from preparations to in vivo MRI applications. J Mater Chem. 2009; 19:6274–6293.

[23]. Weinstein JS, Varallyay CG, Dosa E, Gahramanov S, Hamilton B, Rooney WD, Muldoon LL, Neuwelt EA. Superparamagnetic iron oxide nanoparticles: diagnostic magnetic resonance imaging and potential therapeutic applications in neurooncology and central nervous system inflammatory pathologies, a review. J Cereb Blood Flow Metab. 2010; 30:15–35. [PubMed: 19756021]

[24]. Xu C, Sun S. New forms of superparamagnetic nanoparticles for biomedical applications. Adv Drug Deliv Rev. 2013; 65:732–743. [PubMed: 23123295]

[25]. Laurent S, Forge D, Port M, Roch A, Robic C, Vander Elst L, Muller RN. Magnetic iron oxide nanoparticles: synthesis, stabilization, vectorization, physicochemical characterizations, and biological applications. Chem Rev. 2008; 108:2064–2110. [PubMed: 18543879]

[26]. Iv M, Telischak N, Feng D, Holdsworth SJ, Yeom KW, Daldrup-Link HE. Clinical applications of iron oxide nanoparticles for magnetic resonance imaging of brain tumors. Nanomedicine. 2015; 10:993–1018. [PubMed: 25867862]

[27]. Wáng YXJ, Idée J-M. A comprehensive literatures update of clinical researches of superparamagnetic resonance iron oxide nanoparticles for magnetic resonance imaging. Quant Imaging Med Surg. 2017; 7:88–122. [PubMed: 28275562]

[28]. Hasany S, Ahmed I, Rajan J, Rehman A. Systematic review of the preparation techniques of iron oxide magnetic nanoparticles. J Nanosci Nanotechnol. 2012; 2:148–158.

[29]. Sodipo BK, Aziz AA. Recent advances in synthesis and surface modification of superparamagnetic iron oxide nanoparticles with silica. J Magn Magn Mater. 2016; 416:275–291.

[30]. Remya N, Syama S, Sabareeswaran A, Mohanan P. Toxicity, toxicokinetics and biodistribution of dextran stabilized Iron oxide Nanoparticles for biomedical applications. Int J Pharm. 2016; 511:586–598. [PubMed: 27451271]

[31]. Gupta AK, Gupta M. Synthesis and surface engineering of iron oxide nanoparticles for biomedical applications. Biomaterials. 2005; 26:3995–4021. [PubMed: 15626447]

[32]. Petcharoen K, Sirivat A. Synthesis and characterization of magnetite nanoparticles via the chemical co-precipitation method. Mater Sci Eng B. 2012; 177:421–427.

[33]. Liu Y, Jia S, Wu Q, Ran J, Zhang W, Wu S. Studies of Fe 3 O 4-chitosan nanoparticles prepared by co-precipitation under the magnetic field for lipase immobilization. Catalysis Communications. 2011; 12:717–720.

[34]. Wu S, Sun A, Zhai F, Wang J, Xu W, Zhang Q, Volinsky AA. Fe 3 O 4 magnetic nanoparticles synthesis from tailings by ultrasonic chemical co-precipitation. Materials Letters. 2011; 65:1882–1884.

[35]. Pereira C, Pereira AM, Fernandes C, Rocha M, Mendes R, Fernández-García MP, Guedes A, Tavares PB, Grenèche J-M, Araújo JoP. Superparamagnetic MFe2O4 (M= Fe, Co, Mn) nanoparticles: tuning the particle size and magnetic properties through a novel one-step coprecipitation route. Chemistry of Materials. 2012; 24:1496–1504.

[36]. Suh SK, Yuet K, Hwang DK, Bong KW, Doyle PS, Hatton TA. Synthesis of nonspherical superparamagnetic particles: in situ coprecipitation of magnetic nanoparticles in microgels prepared by stop-flow lithography. Journal of the American Chemical Society. 2012; 134:7337–7343. [PubMed: 22462394]

[37]. Roy E, Patra S, Madhuri R, Sharma PK. Stimuli-responsive poly(N-isopropyl acrylamide)-co-tyrosine@gadolinium: Iron oxide nanoparticle-based nanotheranostic for cancer diagnosis and treatment. Colloids and surfaces B, Biointerfaces. 2016; 142:248–258. [PubMed: 26962761]

[38]. Park J, An K, Hwang Y, Park J-G, Noh H-J, Kim J-Y, Park J-H, Hwang N-M, Hyeon T. Ultra-large-scale syntheses of monodisperse nanocrystals. Nat Mater. 2004; 3:891. [PubMed: 15568032]

[39]. Hufschmid R, Arami H, Ferguson RM, Gonzales M, Teeman E, Brush LN, Browning ND, Krishnan KM. Synthesis of phase-pure and monodisperse iron oxide nanoparticles by thermal decomposition. Nanoscale. 2015; 7:11142–11154. [PubMed: 26059262]

[40]. Sharifi I, Shokrollahi H, Amiri S. Ferrite-based magnetic nanofluids used in hyperthermia applications. J Magn Magn Mate. 2012; 324:903–915.

[41]. Lee Y, Lee J, Bae CJ, Park JG, Noh HJ, Park JH, Hyeon T. Large-scale synthesis of uniform and crystalline magnetite nanoparticles using reverse micelles as nanoreactors under reflux conditions. Advanced functional materials. 2005; 15:503–509.

[42]. Tartaj P, Serna CJ. Microemulsion-assisted synthesis of tunable superparamagnetic composites. Chemistry of materials. 2002; 14:4396–4402.

[43]. Darmawan A, Smart S, Julbe A, Diniz da Costa JC. Iron oxide silica derived from sol-gel synthesis. Materials. 2011; 4:448–456. [PubMed: 28879999]

[44]. Puscasu E, Sacarescu L, Lupu N, Grigoras M, Oanca G, Balasoiu M, Creanga D. Iron oxide-silica nanocomposites yielded by chemical route and sol–gel method. J Sol-Gel Sci Technol. 2016; 79:457–465.

[45]. Fernandes MTC, Garcia RBR, Leite CAP, Kawachi EY. The competing effect of ammonia in the synthesis of iron oxide/silica nanoparticles in microemulsion/sol–gel system. Colloids Surf A. 2013; 422:136–142.

[46]. Wu W, He Q, Jiang C. Magnetic iron oxide nanoparticles: synthesis and surface functionalization strategies. Nanoscale Res Lett. 2008; 3:397. [PubMed: 21749733]

[47]. Sodipo BK, Aziz AA. One minute synthesis of amino-silane functionalized superparamagnetic iron oxide nanoparticles by sonochemical method. Ultrason Sonochem. 2018; 40:837–840. [PubMed: 28946493]

[48]. Kim EH, Ahn Y, Lee HS. Biomedical applications of superparamagnetic iron oxide nanoparticles encapsulated within chitosan. J Alloys Compd. 2007; 434:633–636.

[49]. Ramimoghadam D, Bagheri S, Hamid SBA. Progress in electrochemical synthesis of magnetic iron oxide nanoparticles. J Magn Magn Mater. 2014; 368:207–229.

[50]. Oh JK, Park JM. Iron oxide-based superparamagnetic polymeric nanomaterials: design, preparation, and biomedical application. Prog Polym Sci. 2011; 36:168–189.

[51]. Li L, Mak K, Leung C, Chan K, Chan W, Zhong W, Pong P. Effect of synthesis conditions on the properties of citric-acid coated iron oxide nanoparticles. Microelectron Eng. 2013; 110:329–334.

[52]. Răcuciu M, Creangă D, Airinei A. Citric-acid-coated magnetite nanoparticles for biological applications. Eur Phys J E. 2006; 21:117–121. [PubMed: 17180642]

[53]. Bloemen M, Brullot W, Luong TT, Geukens N, Gils A, Verbiest T. Improved functionalization of oleic acid-coated iron oxide nanoparticles for biomedical applications. J Nanoparticle Res. 2012; 14:1100.

[54]. Zhang L, He R, Gu H-C. Oleic acid coating on the monodisperse magnetite nanoparticles. Appl Surf Sci. 2006; 253:2611–2617.

[55]. Mamani J, Costa-Filho A, Cornejo D, Vieira E, Gamarra L. Synthesis and characterization of magnetite nanoparticles coated with lauric acid. Mater Charact. 2013; 81:28–36.

[56]. Ebrahiminezhad A, Ghasemi Y, Rasoul-Amini S, Barar J, Davaran S. Impact of amino-acid coating on the synthesis and characteristics of iron-oxide nanoparticles (IONs). Bulletin of the Korean Chemical Society. 2012; 33:3957–3962.

[57]. Ahmadi R, Ranjbarnodeh E, Gu N. Synthesizing cysteine-coated magnetite nanoparticles as MRI contrast agent: Effect of pH and cysteine addition on particles size distribution. Materials Science-Poland. 2012; 30:382–389.

[58]. Nosrati H, Hamzehei H, Afroogh S, Ashabi SF, Attari E, Manjili HK. Phenyl alanine & Tyrosine Amino acids Coated Magnetic Nanoparticles: Preparation and Toxicity study. Drug research. 2018

[59]. Mahmoudi M, Serpooshan V. Silver-coated engineered magnetic nanoparticles are promising for the success in the fight against antibacterial resistance threat. ACS Nano. 2012; 6:2656–2664. [PubMed: 22397679]

[60]. Silva SM, Tavallaie R, Sandiford L, Tilley RD, Gooding JJ. Gold coated magnetic nanoparticles: from preparation to surface modification for analytical and biomedical applications. ChemComm. 2016; 52:7528–7540.

[61]. Szpak A, Fiejdasz S, Prendota W, Str^czek T, Kapusta C, Szmyd J, Nowakowska M, Zapotoczny S. T1–T2 dual-modal MRI contrast agents based on superparamagnetic iron oxide nanoparticles with surface attached gadolinium complexes. J Nanoparticle Res. 2014; 16:2678.

[62]. Alwi R, Telenkov S, Mandelis A, Leshuk T, Gu F, Oladepo S, Michaelian K. Silica-coated super paramagnetic iron oxide nanoparticles (SPION) as biocompatible contrast agent in biomedical photoacoustics. Biomed Opt Express. 2012; 3:2500–2509. [PubMed: 23082291]

[63]. Ye F, Laurent S, Fornara A, Astolfi L, Qin J, Roch A, Martini A, Toprak MS, Muller RN, Muhammed M. Uniform mesoporous silica coated iron oxide nanoparticles as a highly efficient, nontoxic MRI T2 contrast agent with tunable proton relaxivities. Contrast Media Mol Imaging. 2012; 7:460–468. [PubMed: 22821880]

[64]. Stefan M, Pana O, Leostean C, Bele C, Silipas D, Senila M, Gautron E. Synthesis and characterization of Fe3O4–TiO2 core-shell nanoparticles. J Appl Phys. 2014; 116

[65]. Tassa C, Shaw SY, Weissleder R. Dextran-coated iron oxide nanoparticles: a versatile platform for targeted molecular imaging, molecular diagnostics, and therapy. Acc Chem Res. 2011; 44:842–852. [PubMed: 21661727]

[66]. Ayala V, Herrera AP, Latorre-Esteves M, Torres-Lugo M, Rinaldi C. Effect of surface charge on the colloidal stability and in vitro uptake of carboxymethyl dextran-coated iron oxide nanoparticles. J Nanoparticle Res. 2013; 15:1874.

[67]. Gaihre B, Khil MS, Lee DR, Kim HY. Gelatin-coated magnetic iron oxide nanoparticles as carrier system: drug loading and in vitro drug release study. Int J Pharm. 2009; 365:180–189. [PubMed: 18790029]

[68]. Ma, H-l; Qi, X-r; Maitani, Y; Nagai, T. Preparation and characterization of superparamagnetic iron oxide nanoparticles stabilized by alginate. Int J Pharm. 2007; 333:177–186. [PubMed: 17074454]

[69]. Castelló J, Gallardo M, Busquets MA, Estelrich J. Chitosan (or alginate)-coated iron oxide nanoparticles: a comparative study. Colloids Surf A. 2015; 468:151–158.

[70]. Unsoy G, Yalcin S, Khodadust R, Gunduz G, Gunduz U. Synthesis optimization and characterization of chitosan-coated iron oxide nanoparticles produced for biomedical applications. J Nanoparticle Res. 2012; 14:964.

[71]. Cole AJ, David AE, Wang J, Galbán CJ, Hill HL, Yang VC. Polyethylene glycol modified, cross-linked starch-coated iron oxide nanoparticles for enhanced magnetic tumor targeting. Biomaterials. 2011; 32:2183–2193. [PubMed: 21176955]

[72]. Vismara E, Bongio C, Coletti A, Edelman R, Serafini A, Mauri M, Simonutti R, Bertini S, Urso E, Assaraf YG. Albumin and Hyaluronic Acid-Coated Superparamagnetic Iron Oxide Nanoparticles Loaded with Paclitaxel for Biomedical Applications. Molecules. 2017; 22:1030.

[73]. Xie J, Wang J, Niu G, Huang J, Chen K, Li X, Chen X. Human serum albumin coated iron oxide nanoparticles for efficient cell labeling. ChemComm. 2010; 46:433–435.

[74]. Huang J, Wang L, Lin R, Wang AY, Yang L, Kuang M, Qian W, Mao H. Casein-coated iron oxide nanoparticles for high MRI contrast enhancement and efficient cell targeting. ACS Appl Mater Interfaces. 2013; 5:4632–4639. [PubMed: 23633522]

[75]. García-Jimeno S, Estelrich J. Ferrofluid based on polyethylene glycol-coated iron oxide nanoparticles: characterization and properties. Colloids Surf A. 2013; 420:74–81.

[76]. Brullot W, Reddy NK, Wouters J, Valev VK, Goderis B, Vermant J, Verbiest T. Versatile ferrofluids based on polyethylene glycol coated iron oxide nanoparticles. J Magn Magn Mater. 2012; 324:1919–1925.

[77]. Larsen EKU, Nielsen T, Wittenborn T, Rydtoft LM, Lokanathan AR, Hansen L, Østergaard L, Kingshott P, Howard KA, Besenbacher F. Accumulation of magnetic iron oxide nanoparticles coated with variably sized polyethylene glycol in murine tumors. Nanoscale. 2012; 4:2352–2361. [PubMed: 22395568]

[78]. Yue-Jian C, Juan T, Fei X, Jia-Bi Z, Ning G, Yi-Hua Z, Ye D, Liang G. Synthesis, self-assembly, and characterization of PEG-coated iron oxide nanoparticles as potential MRI contrast agent. Drug Dev Ind Pharm. 2010; 36:1235–1244. [PubMed: 20818962]

[79]. Huang J, Bu L, Xie J, Chen K, Cheng Z, Li X, Chen X. Effects of nanoparticle size on cellular uptake and liver MRI with polyvinylpyrrolidone-coated iron oxide nanoparticles. ACS Nano. 2010; 4:7151–7160. [PubMed: 21043459]

[80]. Kayal S, Ramanujan R. Doxorubicin loaded PVA coated iron oxide nanoparticles for targeted drug delivery. Mater Sci Eng C. 2010; 30:484–490.

[81]. Wu M, Zhang D, Zeng Y, Wu L, Liu X, Liu J. Nanocluster of superparamagnetic iron oxide nanoparticles coated with poly (dopamine) for magnetic field-targeting, highly sensitive MRI and photothermal cancer therapy. Nanotechnology. 2015; 26:115–102.

[82]. Lin L-S, Cong Z-X, Cao J-B, Ke K-M, Peng Q-L, Gao J, Yang H-H, Liu G, Chen X. Multifunctional Fe3O4@ polydopamine core–shell nanocomposites for intracellular mRNA detection and imaging-guided photothermal therapy. ACS Nano. 2014; 8:3876–3883. [PubMed: 24654734]

[83]. Schleich N, Sibret P, Danhier P, Ucakar B, Laurent S, Muller RN, Jérôme C, Gallez B, Preat V, Danhier F. Dual anticancer drug/superparamagnetic iron oxide-loaded PLGA-based nanoparticles for cancer therapy and magnetic resonance imaging. Int J Pharm. 2013; 447:94–101. [PubMed: 23485340]

[84]. Sun W, Mignani S, Shen M, Shi X. Dendrimer-based magnetic iron oxide nanoparticles: their synthesis and biomedical applications. Drug Discov Today. 2016; 21:1873–1885. [PubMed: 27388223]

[85]. Mojica Pisciotti ML, Lima E Jr, Vasquez Mansilla M, Tognoli V, Troiani HE, Pasa A, Creczynski-Pasa T, Silva A, Gurman P, Colombo L. In vitro and in vivo experiments with iron oxide nanoparticles functionalized with DEXTRAN or polyethylene glycol for medical applications: magnetic targeting. Journal of Biomedical Materials Research Part B: Applied Biomaterials. 2014; 102:860–868.

[86]. Yu M, Huang S, Yu KJ, Clyne AM. Dextran and polymer polyethylene glycol (PEG) coating reduce both 5 and 30 nm iron oxide nanoparticle cytotoxicity in 2D and 3D cell culture. Int J Mol Sci. 2012; 13:5554–5570. [PubMed: 22754315]

[87]. Wang Y-XJ. Superparamagnetic iron oxide based MRI contrast agents: Current status of clinical application. Quant Imaging Med Surg. 2011; 1:35. [PubMed: 23256052]

[88]. Vega-Chacón J, Arbeláez MIA, Jorge JH, Marques RFC, Jafelicci M Jr. pH-responsive poly (aspartic acid) hydrogel-coated magnetite nanoparticles for biomedical applications. Mater Sci Eng C. 2017; 77:366–373.

[89]. Cheng R, Meng F, Deng C, Klok H-A, Zhong Z. Dual and multi-stimuli responsive polymeric nanoparticles for programmed site-specific drug delivery. Biomaterials. 2013; 34:3647–3657. [PubMed: 23415642]

[90]. Yang H-M, Oh BC, Kim JH, Ahn T, Nam H-S, Park CW, Kim J-D. Multifunctional poly (aspartic acid) nanoparticles containing iron oxide nanocrystals and doxorubicin for simultaneous cancer diagnosis and therapy. Colloids Surf A. 2011; 391:208–215.

[91]. Medeiros SF, Santos AM, Fessi H, Elaissari A. Thermally-sensitive and magnetic poly (N-vinylcaprolactam)-based nanogels by inverse miniemulsion polymerization. J Coll Sci Biotech. 2012; 1:99–112.

[92]. Wei W, Qi X, Liu Y, Li J, Hu X, Zuo G, Zhang J, Dong W. Synthesis and characterization of a novel pH-thermo dual responsive hydrogel based on salecan and poly (N, N-diethylacrylamide-co-methacrylic acid). Colloids Surf B. 2015; 136:1182–1192.

[93]. Kamoun EA, Fahmy A, Taha TH, El-Fakharany EM, Makram M, Soliman HM, Shehata H. Thermo- and pH-sensitive hydrogel membranes composed of poly (N-isopropylacrylamide)-hyaluronan for biomedical applications: Influence of hyaluronan incorporation on the membrane properties. Int J Biol Macromol. 2018; 106:158–167. [PubMed: 28780413]

[94]. Fortin-Ripoche J-P, Martina MS, Gazeau F, Ménager C, Wilhelm C, Bacri J-C, Lesieur S, Clement O. Magnetic targeting of magnetoliposomes to solid tumors with MR imaging monitoring in mice: feasibility. Radiology. 2006; 239:415–424. [PubMed: 16549622]

[95]. Nappini S, Bombelli FB, Bonini M, Nordèn B, Baglioni P. Magnetoliposomes for controlled drug release in the presence of low-frequency magnetic field. Soft Matter. 2010; 6:154–162.

[96]. Amstad E, Kohlbrecher J, Müller E, Schweizer T, Textor M, Reimhult E. Triggered release from liposomes through magnetic actuation of iron oxide nanoparticle containing membranes. Nano letters. 2011; 11:1664–1670. [PubMed: 21351741]

[97]. Tai L-A, Tsai P-J, Wang Y-C, Wang Y-J, Lo L-W, Yang C-S. Thermosensitive liposomes entrapping iron oxide nanoparticles for controllable drug release. Nanotechnology. 2009; 20

[98]. Hu J, Qian Y, Wang X, Liu T, Liu S. Drug-loaded and superparamagnetic iron oxide nanoparticle surface-embedded amphiphilic block copolymer micelles for integrated chemotherapeutic drug delivery and MR imaging. Langmuir. 2011; 28:2073–2082. [PubMed: 22047551]

[99]. Nasongkla N, Bey E, Ren J, Ai H, Khemtong C, Guthi JS, Chin S-F, Sherry AD, Boothman DA, Gao J. Multifunctional polymeric micelles as cancer-targeted, MRI-ultrasensitive drug delivery systems. Nano letters. 2006; 6:2427–2430. [PubMed: 17090068]

[100]. Ai H, Flask C, Weinberg B, Shuai XT, Pagel MD, Farrell D, Duerk J, Gao J. Magnetite-loaded polymeric micelles as ultrasensitive magnetic-resonance probes. Advanced Materials. 2005; 17

[101]. Talelli M, Rijcken CJ, Lammers T, Seevinck PR, Storm G, van Nostrum CF, Hennink WE. Superparamagnetic iron oxide nanoparticles encapsulated in biodegradable thermosensitive polymeric micelles: toward a targeted nanomedicine suitable for image-guided drug delivery. Langmuir. 2009; 25:2060–2067. [PubMed: 19166276]

[102]. Bulte JW, De Cuyper M, Despres D, Frank JA. Preparation, relaxometry, and biokinetics of PEGylated magnetoliposomes as MR contrast agent. Journal of Magnetism and Magnetic Materials. 1999; 194:204–209.

[103]. Ali A, Hira Zafar MZ, ul Haq I, Phull AR, Ali JS, Hussain A. Synthesis, characterization, applications, and challenges of iron oxide nanoparticles. Nanotechnol Sci Appl. 2016; 9:49. [PubMed: 27578966]

[104]. Hajba L, Guttman A. The use of magnetic nanoparticles in cancer theranostics: Toward handheld diagnostic devices. Biotechnol Adv. 2016; 34:354–361. [PubMed: 26853617]

[105]. Woo K, Hong J, Choi S, Lee H-W, Ahn J-P, Kim CS, Lee SW. Easy synthesis and magnetic properties of iron oxide nanoparticles. Chem Mater. 2004; 16:2814–2818.

[106]. Mahajan S, Koul V, Choudhary V, Shishodia G, Bharti AC. Preparation and in vitro evaluation of folate-receptor-targeted SPION–polymer micelle hybrids for MRI contrast enhancement in cancer imaging. Nanotechnology. 2012; 24

[107]. Filipe V, Hawe A, Jiskoot W. Critical evaluation of Nanoparticle Tracking Analysis (NTA) by NanoSight for the measurement of nanoparticles and protein aggregates. Pharm Res. 2010; 27:796–810. [PubMed: 20204471]

[108]. Li T, Senesi AJ, Lee B. Small angle X-ray scattering for nanoparticle research. Chem Rev. 2016; 116:11128–11180. [PubMed: 27054962]

[109]. Smolensky ED, Park H-YE, Zhou Y, Rolla GA, Marjńanska M, Botta M, Pierre VC. Scaling laws at the nanosize: the effect of particle size and shape on the magnetism and relaxivity of iron oxide nanoparticle contrast agents. Journal of Materials Chemistry B. 2013; 1:2818–2828. [PubMed: 23819021]

[110]. Blanco-Andujar C, Walter A, Cotin G, Bordeianu C, Mertz D, Felder-Flesch D, Begin-Colin S. Design of iron oxide-based nanoparticles for MRI and magnetic hyperthermia. Nanomedicine. 2016; 11:1889–1910. [PubMed: 27389703]

[111]. Bulte JW, Kraitchman DL. Iron oxide MR contrast agents for molecular and cellular imaging. NMR in Biomedicine. 2004; 17:484–499. [PubMed: 15526347]

[112]. Bulte JW. In vivo MRI cell tracking: clinical studies. American Journal of Roentgenology. 2009; 193:314–325. [PubMed: 19620426]

[113]. Schmale I, Rahmer J, Gleich B, Borgert J, Weizenecker J. Point spread function analysis of magnetic particles. Magnetic Particle Imaging, Springer. 2012:287–292.

[114]. Panagiotopoulos N, Duschka RL, Ahlborg M, Bringout G, Debbeler C, Graeser M, Kaethner C, Lüdtke-Buzug K, Medimagh H, Stelzner J, Buzug TM, Barkhausen J, Vogt FM, Haegele J. Magnetic particle imaging: current developments and future directions. Int J Nanomedicine. 2015; 10:3097–3114. [PubMed: 25960650]

[115]. Guardia P, Di Corato R, Lartigue L, Wilhelm C, Espinosa A, Garcia-Hernandez M, Gazeau F, Manna L, Pellegrino T. Water-soluble iron oxide nanocubes with high values of specific absorption rate for cancer cell hyperthermia treatment. ACS Nano. 2012; 6:3080–3091. [PubMed: 22494015]

[116]. Latunde-Dada GO. Ferroptosis: role of lipid peroxidation, iron and ferritinophagy. Biochimica et Biophysica Acta (BBA)-General Subjects. 2017; 1861:1893–1900. [PubMed: 28552631]

[117]. Brüne B, Dehne N, Grossmann N, Jung M, Namgaladze D, Schmid T, von Knethen A. Weigert A: Redox control of inflammation in macrophages. Antioxidants & redox signaling. 2013; 19:595–637. [PubMed: 23311665]

[118]. Tan H-Y, Wang N, Li S, Hong M, Wang X, Feng Y. The reactive oxygen species in macrophage polarization: reflecting its dual role in progression and treatment of human diseases. Oxid Med Cell Longev. 2016; 2016

[119]. Ankamwar B, Lai T-C, Huang J-H, Liu R-S, Hsiao M, Chen C-H, Hwu Y. Biocompatibility of Fe3O4 nanoparticles evaluated by in vitro cytotoxicity assays using normal, glia and breast cancer cells. Nanotechnology. 2010; 21

[120]. Singh N, Jenkins GJ, Asadi R, Doak SH. Potential toxicity of superparamagnetic iron oxide nanoparticles (SPION). Nano reviews. 2010; 1:5358.

[121]. Liu G, Gao J, Ai H, Chen X. Applications and potential toxicity of magnetic iron oxide nanoparticles. Small. 2013; 9:1533–1545. [PubMed: 23019129]

[122]. Mahmoudi M, Simchi A, Imani M, Shokrgozar MA, Milani AS, Häfeli UO, Stroeve P. A new approach for the in vitro identification of the cytotoxicity of superparamagnetic iron oxide nanoparticles. Colloids and Surfaces, B: Biointerfaces. 2010; 75:300–309. [PubMed: 19781921]

[123]. Xia T, Kovochich M, Liong M, Meng H, Kabehie S, George S, Zink JI, Nel AE. Polyethyleneimine coating enhances the cellular uptake of mesoporous silica nanoparticles and allows safe delivery of siRNA and DNA constructs. ACS Nano. 2009; 3:3273–3286. [PubMed: 19739605]

[124]. Mulens-Arias V, Rojas JM, Pérez-Yagüe S, Morales MP, Barber DF. Polyethylenimine-coated SPIONs trigger macrophage activation through TLR-4 signaling and ROS production and modulate podosome dynamics. Biomaterials. 2015; 52:494–506. [PubMed: 25818455]

[125]. Blank F, Gerber P, Rothen-Rutishauser B, Sakulkhu U, Salaklang J, De Peyer K, Gehr P, Nicod LP, Hofmann H, Geiser T. Biomedical nanoparticles modulate specific CD4+ T cell stimulation

Europe PMC Funders Author Manuscripts

by inhibition of antigen processing in dendritic cells. Nanotoxicology. 2011; 5:606–621. [PubMed: 21231795]

[126]. de Vries IJ, Lesterhuis WJ, Barentsz JO, Verdijk P, van Krieken JH, Boerman OC, Oyen WJ, Bonenkamp JJ, Boezeman JB, Adema GJ, Bulte JW, et al. Magnetic resonance tracking of dendritic cells in melanoma patients for monitoring of cellular therapy. Nat Biotechnol. 2005; 23:1407–1413. [PubMed: 16258544]

[127]. Arbab AS, Yocum GT, Rad AM, Khakoo AY, Fellowes V, Read EJ, Frank JA. Labeling of cells with ferumoxides–protamine sulfate complexes does not inhibit function or differentiation capacity of hematopoietic or mesenchymal stem cells. NMR in Biomedicine: An International Journal Devoted to the Development and Application of Magnetic Resonance In vivo. 2005; 18:553–559.

[128]. Schmidtke-Schrezenmeier G, Urban M, Musyanovych A, Mailänder V, Rojewski M, Fekete N, Menard C, Deak E, Tarte K, Rasche V. Labeling of mesenchymal stromal cells with iron oxide–poly (L-lactide) nanoparticles for magnetic resonance imaging: uptake, persistence, effects on cellular function and magnetic resonance imaging properties. Cytotherapy. 2011; 13:962–975. [PubMed: 21492060]

[129]. Matuszak J, Zaloga J, Friedrich RP, Lyer S, Nowak J, Odenbach S, Alexiou C, Cicha I. Endothelial biocompatibility and accumulation of SPION under flow conditions. J Magn Magn Mater. 2015; 380:2026.

[130]. Polyak B, Fishbein I, Chorny M, Alferiev I, Williams D, Yellen B, Friedman G, Levy RJ. High field gradient targeting of magnetic nanoparticle-loaded endothelial cells to the surfaces of steel stents. PNAS. 2008; 105:698–703. [PubMed: 18182491]

[131]. Pawelczyk E, Arbab AS, Pandit S, Hu E, Frank JA. Expression of transferrin receptor and ferritin following ferumoxides–protamine sulfate labeling of cells: implications for cellular magnetic resonance imaging. NMR in Biomedicine: An International Journal Devoted to the Development and Application of Magnetic Resonance In vivo. 2006; 19:581–592.

[132]. Weissleder R, Nahrendorf M, Pittet MJ. Imaging macrophages with nanoparticles. Nat Mater. 2014; 13:125. [PubMed: 24452356]

[133]. Rizzo LY, Golombek SK, Mertens ME, Pan Y, Laaf D, Broda J, Jayapaul J, Möckel D, Subr V, Hennink WE. In vivo nanotoxicity testing using the zebrafish embryo assay. Journal of Materials Chemistry B. 2013; 1:3918–3925.

[134]. Hamm B, Staks T, Taupitz M, Maibauer R, Speidel A, Huppertz A, Frenzel T, Lawaczeck R, Wolf KJ, Lange L. Contrast-enhanced MR imaging of liver and spleen: first experience in humans with a new superparamagnetic iron oxide. J Magn Reson Imaging. 1994; 4:659–668. [PubMed: 7981510]

[135]. Bernd H, De Kerviler E, Gaillard S, Bonnemain B. Safety and tolerability of ultrasmall superparamagnetic iron oxide contrast agent: comprehensive analysis of a clinical development program. Invest Radiol. 2009; 44:336–342. [PubMed: 19661843]

[136]. Toth GB, Varallyay CG, Horvath A, Bashir MR, Choyke PL, Daldrup-Link HE, Dosa E, Finn JP, Gahramanov S, Harisinghani M. Current and potential imaging applications of ferumoxytol for magnetic resonance imaging. Kidney Int. 2017; 92:47–66. [PubMed: 28434822]

[137]. Chen F, Ward J, Robinson P. MR imaging of the liver and spleen: a comparison of the effects on signal intensity of two superparamagnetic iron oxide agents. Magn Imaging Reson. 1999; 17:549–556.

[138]. Choi J-Y, Kim M-J, Kim JH, Kim SH, Ko H-K, Lim JS, Oh YT, Chung J-J, Yoo HS, Lee JT. Detection of hepatic metastasis: manganese-and ferucarbotran-enhanced MR imaging. Eur J Radiol. 2006; 60:84–90. [PubMed: 16920315]

[139]. Wang Y-XJ, Hussain SM, Krestin GP. Superparamagnetic iron oxide contrast agents: physicochemical characteristics and applications in MR imaging. Eur Radiol. 2001; 11:2319–2331. [PubMed: 11702180]

[140]. Neuwelt A, Sidhu N, Hu C-AA, Mlady G, Eberhardt SC, Sillerud LO. Iron-Based Superparamagnetic Nanoparticle Contrast Agents for MRI of Infection and Inflammation. Am J Roentgenol. 2015; 204:W302–W313. [PubMed: 25714316]

[141]. Tromsdorf UI, Bruns OT, Salmen SC, Beisiegel U, Weller H. A highly effective, nontoxic T 1 MR contrast agent based on ultrasmall PEGylated iron oxide nanoparticles. Nano Lett. 2009; 9:4434–4440. [PubMed: 19799448]

[142]. Hu F, Jia Q, Li Y, Gao M. Facile synthesis of ultrasmall PEGylated iron oxide nanoparticles for dual-contrast T1- and T2-weighted magnetic resonance imaging. Nanotechnology. 2011; 22

[143]. Kiessling F, Mertens ME, Grimm J, Lammers T. Nanoparticles for Imaging: Top or Flop? Radiology. 2014; 273:10–28. [PubMed: 25247562]

[144]. Marchal G, Van Hecke P, Demaerel P, Decrop E, Kennis C, Baert A, van der Schueren E. Detection of liver metastases with superparamagnetic iron oxide in 15 patients: results of MR imaging at 1.5 T. Am J Roentgenol. 1989; 152:771–775. [PubMed: 2784260]

[145]. Ferrucci JT, Stark DD. Iron oxide-enhanced MR imaging of the liver and spleen: review of the first 5 years. Am J Roentgenol. 1990; 155:943–950. [PubMed: 2120963]

[146]. Liver MR imaging with iron oxides: toward consensus and clinical practice. Radiology.

[147]. Reimer P, Balzer T. Ferucarbotran (Resovist): a new clinically approved RES-specific contrast agent for contrast-enhanced MRI of the liver: properties, clinical development, and applications. Eur Radiol. 2003; 13:1266–1276. [PubMed: 12764641]

[148]. Chen F, Ward J, Robinson PJ. MR imaging of the liver and spleen: a comparison of the effects on signal intensity of two superparamagnetic iron oxide agents. Magn Imaging Reson. 1999; 17:549–556.

[149]. Santoro L, Grazioli L, Filippone A, Grassedonio E, Belli G, Colagrande S. Resovist enhanced MR imaging of the liver: does quantitative assessment help in focal lesion classification and characterization? J Magn Imaging Reson. 2009; 30:1012–1020.

[150]. Matsuo M, Kanematsu M, Itoh K, Murakami T, Maetani Y, Kondo H, Goshima S, Kako N, Hoshi H, Konishi J, Moriyama N, et al. Detection of Malignant Hepatic Tumors with Ferumoxides-Enhanced, MRI: Comparison of Five Gradient-Recalled Echo Sequences with Different TEs. Am J Roentgenol. 2004; 182:235–242. [PubMed: 14684545]

[151]. Chanyaputhipong J, Low S-CA, Chow PKH. Gadoxetate Acid-Enhanced MR Imaging for HCC: A Review for Clinicians. Int J Hepatol. 2011; 2011

[152]. Thian YL, Riddell AM, Koh D-M. Liver-specific agents for contrast-enhanced MRI: role in oncological imaging. Cancer Imaging. 2013; 13:567–579. [PubMed: 24434892]

[153]. MP A. Diagnostic accuracy of MR colonography with fecal tagging.

[154]. Neuwelt EA, Hamilton BE, Varallyay CG, Rooney WR, Edelman RD, Jacobs PM, Watnick SG. Ultrasmall superparamagnetic iron oxides (USPIOs): a future alternative magnetic resonance (MR) contrast agent for patients at risk for nephrogenic systemic fibrosis (NSF)? Kidney Int. 2009; 75:465–474. [PubMed: 18843256]

[155]. Torabi M, Aquino SL, Harisinghani MG. Current Concepts in Lymph Node Imaging. J Nucl Med. 2004; 45:1509–1518. [PubMed: 15347718]

[156]. Bremerich J, Bilecen D, Reimer P. MR angiography with blood pool contrast agents. European Radiology. 2007; 17:3017. [PubMed: 17639407]

[157]. Fortuin, Ansje S; Brüggemann, R; Linden, J; Panfilov, I; Israël, B; Scheenen, Tom WJ; Barentsz, Jelle O. Ultra-small superparamagnetic iron oxides for metastatic lymph node detection: back on the block. Wiley Interdiscip Rev Nanomed Nanobiotechnol. 2017; 10:e1471.

[158]. Turkbey B, Agarwal HK, Shih J, Bernardo M, McKinney YL, Daar D, Griffiths GL, Sankineni S, Johnson L, Grant KB, Weaver J, et al. A Phase I Dosing Study of Ferumoxytol for MR Lymphography at 3 T in Patients With Prostate Cancer. Am J Roentgenol. 2015; 205:64–69. [PubMed: 26102381]

[159]. Vassallo P, Matei C, Heston WD, McLachlan SJ, Koutcher JA, Castellino RA. AMI-227-enhanced MR lymphography: usefulness for differentiating reactive from tumor-bearing lymph nodes. Radiology. 1994; 193:501–506. [PubMed: 7972768]

[160]. Fortuin AS, Deserno WMLLG, Meijer HJM, Jager GJ, Takahashi S, Debats OA, Reske SN, Schick C, Krause BJ, van Oort I, Witjes AJ, et al. Value of PET/CT and MR Lymphography in Treatment of Prostate Cancer Patients With Lymph Node Metastases. International Journal of Radiation Oncology*Biology*Physics. 2012; 84:712–718.

[161]. Harisinghani MG, Barentsz J, Hahn PF, Deserno WM, Tabatabaei S, van de Kaa CH, de la Rosette J, Weissleder R. Noninvasive Detection of Clinically Occult Lymph-Node Metastases in Prostate Cancer. N Engl J Med. 2003; 348:2491–2499. [PubMed: 12815134]

[162]. Heesakkers RAM, Hövels AM, Jager GJ, van den Bosch HCM, Witjes JA, Raat HPJ, Severens JL, Adang EMM, van der Kaa CH, Fütterer JJ, Barentsz J. MRI with a lymph-node-specific contrast agent as an alternative to CT scan and lymph-node dissection in patients with prostate cancer: a prospective multicohort study. The Lancet Oncology. 2008; 9:850–856. [PubMed: 18708295]

[163]. Kimura K, Tanigawa N, Matsuki M, Nohara T, Iwamoto M, Sumiyoshi K, Tanaka S, Takahashi Y, Narumi Y. High-resolution MR lymphography using ultrasmall superparamagnetic iron oxide (USPIO) in the evaluation of axillary lymph nodes in patients with early stage breast cancer: preliminary results. Breast Cancer. 2010; 17:241–246. [PubMed: 19575282]

[164]. Pultrum BB, van der Jagt EJ, van Westreenen HL, van Dullemen HM, Kappert P, Groen H, Sietsma J, Oudkerk M, Plukker JTM, van Dam GM. Detection of lymph node metastases with ultrasmall superparamagnetic iron oxide (USPIO)-enhanced magnetic resonance imaging in oesophageal cancer: a feasibility study. Cancer Imaging: The Official Publication of the International Cancer Imaging Society. 2009; 9:19–28. [PubMed: 19414293]

[165]. Thoeny HC, Froehlich JM, Triantafyllou M, Huesler J, Bains LJ, Vermathen P, Fleischmann A, Studer UE. Metastases in normal-sized pelvic lymph nodes: detection with diffusion-weighted MR imaging. Radiology. 2014; 273:125–135. [PubMed: 24893049]

[166]. Mack MG, Balzer JO, Straub R, Eichler K, Vogl TJ. Superparamagnetic iron oxide-enhanced MR imaging of head and neck lymph nodes. Radiology. 2002; 222:239–244. [PubMed: 11756732]

[167]. Triantafyllou M, Studer UE, Birkhäuser FD, Fleischmann A, Bains LJ, Petralia G, Christe A, Froehlich JM, Thoeny HC. Ultrasmall superparamagnetic particles of iron oxide allow for the detection of metastases in normal sized pelvic lymph nodes of patients with bladder and/or prostate cancer. European Journal of Cancer (Oxford, England: 1990). 2013; 49:616–624.

[168]. Karabulut N, Elmas N. Contrast agents used in MR imaging of the liver. Diagn Interv Radiol. 2006; 12:22–30. [PubMed: 16538580]

[169]. Weissleder R, Nahrendorf M, M.Pittet J. Imaging macrophages with nanoparticles. Nat Mater. 2014; 13:125–138. [PubMed: 24452356]

[170]. Lobatto ME, Fuster V, Fayad ZA, Mulder WJ. Perspectives and opportunities for nanomedicine in the management of atherosclerosis. Nat Rev Drug Discov. 2011; 10:835–852. [PubMed: 22015921]

[171]. Kaneko C, Nitta N, Tsuchiya K, Watanabe S, Nitta-Seko A, Ohta S, Otani H, Sonoda A, Murata K, Shiomi M. MRI study of atherosclerotic plaque progression using ultrasmall superparamagnetic iron oxide in Watanabe heritable hyperlipidemic rabbits. Brit J Radiol. 2015; 88

[172]. Kooi ME, Cappendijk VC, Cleutjens KBJM, Kessels AGH, Kitslaar PJEHM, Borgers M, Frederik PM, Daemen MJaP, Engelshoven JMAv. Accumulation of Ultrasmall Superparamagnetic Particles of Iron Oxide in Human Atherosclerotic Plaques Can Be Detected by In Vivo Magnetic Resonance Imaging. Circulation. 2003; 107:2453–2458. [PubMed: 12719280]

[173]. Trivedi RA, Mallawarachi C, U-King-Im J-M, Graves MJ, Horsley J, Goddard MJ, Brown A, Wang L, Kirkpatrick PJ, Brown J, Gillard JH. Identifying inflamed carotid plaques using in vivo USPIO-enhanced MR imaging to label plaque macrophages. Arterioscler Thromb Vasc Biol. 2006; 26

[174]. Swirski FK, Nahrendorf M. Imaging macrophage development and fate in atherosclerosis and myocardial infarction. Immunol Cell Biol. 2013; 91:297–303. [PubMed: 23207281]

[175]. Tourdias T, Roggerone S, Filippi M, Kanagaki M, Rovaris M, Miller DH, Petry KG, Brochet B, Pruvo J-P, Radue E-W, Dousset V. Assessment of Disease Activity in Multiple Sclerosis Phenotypes with Combined Gadolinium- and Superparamagnetic Iron Oxide–enhanced MR Imaging. Radiology. 2012; 264:225–233. [PubMed: 22723563]

[176]. Vellinga MM, Engberink O, D R, Seewann A, Pouwels PJW, Wattjes MP, Pol VD, S Ma, Pering C, Polman CH, Vries D, et al. Pluriformity of inflammation in multiple sclerosis shown by ultra-small iron oxide particle enhancement. Brain. 2008; 131:800–807. [PubMed: 18245785]

[177]. Maarouf A, Ferré J-C, Zaaraoui W, Le Troter A, Bannier E, Berry I, Guye M, Pierot L, Barillot C, Pelletier J, Tourbah A, et al. Ultra-small superparamagnetic iron oxide enhancement is associated with higher loss of brain tissue structure in clinically isolated syndrome. Mult Scler J. 2016; 22:1032–1039.

[178]. Gaglia JL, Guimaraes AR, Harisinghani M, Turvey SE, Jackson R, Benoist C, Mathis D, Weissleder R. Noninvasive imaging of pancreatic islet inflammation in type 1A diabetes patients. J Clin Invest. 2011; 121:442–445. [PubMed: 21123946]

[179]. Schnorr J, Wagner S, Abramjuk C, Wojner I, Schink T, Kroencke TJ, Schellenberger E, Hamm B, Pilgrimm H, Taupitz M. Comparison of the iron oxide-based blood-pool contrast medium VSOP-C184 with gadopentetate dimeglumine for first-pass magnetic resonance angiography of the aorta and renal arteries in pigs. Invest Radiol. 2004; 39:546–553. [PubMed: 15308937]

[180]. Taupitz M, Wagner S, Schnorr J, Kravec I, Pilgrimm H, Bergmann-Fritsch H, Hamm B. Phase I clinical evaluation of citrate-coated monocrystalline very small superparamagnetic iron oxide particles as a new contrast medium for magnetic resonance imaging. Invest Radiol. 2004; 39:394–405. [PubMed: 15194910]

[181]. Goyen M. Gadofosveset-enhanced magnetic resonance angiography. Vasc Health Risk Manag. 2008; 4:1–9. [PubMed: 18629367]

[182]. Ersoy H, Jacobs P, Kent CK, Prince MR. Blood Pool MR Angiography of Aortic Stent-Graft Endoleak. Am J Roentgenol. 2004; 182:1181–1186. [PubMed: 15100115]

[183]. Sakuma H. Coronary CT versus MR Angiography: The Role of MR Angiography. Radiology. 2011; 258:340–349. [PubMed: 21273518]

[184]. Klein C, Schalla S, Schnackenburg B, Bornstedt A, Hoffmann V, Fleck E, Nagel E. Improvement of image quality of non-invasive coronary artery imaging with magnetic resonance by the use of the intravascular contrast agent Clariscan™ (NC100150 injection) in patients with coronary artery disease. J Magn Reson Imaging. 2003; 17:656–662. [PubMed: 12766894]

[185]. Bedaux WL, Hofman MB, Wielopolski PA, de Cock CC, Hoffmann V, Oudkerk M, de Feyter PJ, van Rossum AC. Three-dimensional magnetic resonance coronary angiography using a new blood pool contrast agent: initial experience. J Cardiovasc Magn Reson. 2002; 4:273–282. [PubMed: 12074142]

[186]. Larsson E-M, Sundén P, Olsson C-G, Debatin J, Duerinckx AJ, Baum R, Hahn D, Ebner F. MR Venography Using an Intravascular Contrast Agent: Results from a Multicenter Phase 2 Study of Dosage. Am J Roentgenol. 2003; 180:227–232. [PubMed: 12490510]

[187]. Perazella MA. Current status of gadolinium toxicity in patients with kidney disease. Clinical journal of the American Society of Nephrology: CJASN. 2009; 4:461–469. [PubMed: 19201920]

[188]. Sigovan M, Gasper W, Alley HF, Owens CD, Saloner D. USPIO-enhanced MR angiography of arteriovenous fistulas in patients with renal failure. Radiology. 2012; 265:584–590. [PubMed: 22875796]

[189]. Corwin MT, Fananapazir G, Chaudhari AJ. MR Angiography of Renal Transplant Vasculature with Ferumoxytol: Comparison of High-Resolution Steady-State and First-Pass Acquisitions. Acad Radiol. 2016; 23:368–373. [PubMed: 26707344]

[190]. Hamilton BE, Nesbit GM, Dosa E, Gahramanov S, Rooney B, Nesbit EG, Raines J, Neuwelt EA. Comparative Analysis of Ferumoxytol and Gadoteridol Enhancement Using T1- and T2-Weighted MRI in Neuroimaging. Am J Roentgenol. 2011; 197:981–988. [PubMed: 21940589]

[191]. Gahramanov S, Muldoon LL, Varallyay CG, Li X, Kraemer DF, Fu R, Hamilton BE, Rooney WD, Neuwelt EA. Pseudoprogression of glioblastoma after chemo- and radiation therapy: diagnosis by using dynamic susceptibility-weighted contrast-enhanced perfusion MR imaging with ferumoxytol versus gadoteridol and correlation with survival. Radiology. 2013; 266:842–852. [PubMed: 23204544]

[192]. McDonald RJ, McDonald JS, Kallmes DF, Jentoft ME, Murray DL, Thielen KR, Williamson EE, Eckel LJ. Intracranial Gadolinium Deposition after Contrast-enhanced MR Imaging. Radiology. 2015; 275:772–782. [PubMed: 25742194]

[193]. Pablico-Lansigan MH, Situ SF, Samia ACS. Magnetic particle imaging: advancements and perspectives for real-time in vivo monitoring and image-guided therapy. Nanoscale. 2013; 5:4040–4055. [PubMed: 23538400]

[194]. Kaul MG, Weber O, Heinen U, Reitmeier A, Mummert T, Jung C, Raabe N, Knopp T, Ittrich H, Adam G. Combined Preclinical Magnetic Particle Imaging and Magnetic Resonance Imaging: Initial Results in Mice. RoFo: Fortschritte Auf Dem Gebiete Der Rontgenstrahlen Und Der Nuklearmedizin. 2015; 187:347–352. [PubMed: 25962671]

[195]. Vogel P, Rückert MA, Klauer P, Kullmann WH, Jakob PM, Behr VC. First in vivo traveling wave magnetic particle imaging of a beating mouse heart. Phys Med Biol. 2016; 61:6620. [PubMed: 27541258]

[196]. Kratz H, Taupitz M, Schellenberger AAd, Kosch O, Eberbeck D, Wagner S, Trahms L, Hamm B, Schnorr J. Novel magnetic multicore nanoparticles designed for MPI and other biomedical applications: From synthesis to first in vivo studies. PLoS One. 2018; 13:e0190214. [PubMed: 29300729]

[197]. Haegele J, Rahmer J, Gleich B, Borgert J, Wojtczyk H, Panagiotopoulos N, Buzug TM, Barkhausen J, Vogt FM. Magnetic Particle Imaging: Visualization of Instruments for Cardiovascular Intervention. Radiology. 2012; 265:933–938. [PubMed: 22996744]

[198]. Zheng B, Vazin T, Goodwill PW, Conway A, Verma A, Saritas EU, Schaffer D, Conolly SM. Magnetic Particle Imaging tracks the long-term fate of in vivo neural cell implants with high image contrast. Sci Rep. 2015; 5

[199]. Tay ZW, Chandrasekharan P, Chiu-Lam A, Hensley DW, Dhavalikar R, Zhou XY, Yu EY, Goodwill PW, Zheng B, Rinaldi C, Conolly SM. Magnetic Particle Imaging-Guided Heating in Vivo Using Gradient Fields for Arbitrary Localization of Magnetic Hyperthermia Therapy. ACS Nano. 2018; 12

[200]. Zheng B, von See MP, Yu E, Gunel B, Lu K, Vazin T, Schaffer DV, Goodwill PW, Conolly SM. Quantitative Magnetic Particle Imaging Monitors the Transplantation, Biodistribution, and Clearance of Stem Cells In Vivo. Theranostics. 2016; 6:291–301. [PubMed: 26909106]

[201]. Plouffe BD, Murthy SK, Lewis LH. Fundamentals and Application of Magnetic Particles in Cell Isolation and Enrichment. Rep Prog Phys. 2015; 78

[202]. Mi Y, Li K, Liu Y, Pu K-Y, Liu B, Feng S-S. Herceptin functionalized polyhedral oligomeric silsesquioxane – conjugated oligomers – silica/iron oxide nanoparticles for tumor cell sorting and detection. Biomaterials. 2011; 32:8226–8233. [PubMed: 21816464]

[203]. Xu H, Aguilar ZP, Yang L, Kuang M, Duan H, Xiong Y, Wei H, Wang A. Antibody conjugated magnetic iron oxide nanoparticles for cancer cell separation in fresh whole blood. Biomaterials. 2011; 32:9758–9765. [PubMed: 21920599]

[204]. Perez JM, O'Loughin T, Simeone FJ, Weissleder R, Josephson L. DNA-Based Magnetic Nanoparticle Assembly Acts as a Magnetic Relaxation Nanoswitch Allowing Screening of DNA-Cleaving Agents. J Am Chem Soc. 2002; 124:2856–2857. [PubMed: 11902860]

[205]. Lee H, Sun E, Ham D, Weissleder R. Chip-NMR biosensor for detection and molecular analysis of cells. Nat Med. 2008; 14:869–874. [PubMed: 18607350]

[206]. Perez JM, Josephson L, Weissleder R. Use of Magnetic Nanoparticles as Nanosensors to Probe for Molecular Interactions. Chembiochem. 2004; 5:261–264. [PubMed: 14997516]

[207]. Perez JM, Josephson L, O'Loughlin T, Hogemann D, Weissleder R. Magnetic relaxation switches capable of sensing molecular interactions. Nat Biotechnol. 2002; 20:816–820. [PubMed: 12134166]

[208]. Wildgruber M, Lee H, Chudnovskiy A, Yoon T-J, Etzrodt M, Pittet MJ, Nahrendorf M, Croce K, Libby P, Weissleder R, Swirski FK. Monocyte Subset Dynamics in Human Atherosclerosis Can Be Profiled with Magnetic Nano-Sensors. PLoS One. 2009; 4:e5663. [PubMed: 19461894]

[209]. Coyne DW. Ferumoxytol for treatment of iron deficiency anemia in patients with chronic kidney disease. Expert Opin Pharmacother. 2009; 10:2563–2568. [PubMed: 19708851]

[210]. Sica A, Allavena P, Mantovani A. Cancer related inflammation: the macrophage connection. Cancer Lett. 2008; 267:204–215. [PubMed: 18448242]

[211]. Costa da Silva M, Breckwoldt MO, Vinchi F, Correia MP, Stojanovic A, Thielmann CM, Meister M, Muley T, Warth A, Platten M, Hentze MW, et al. Iron Induces Anti-tumor Activity in Tumor-Associated Macrophages. Front Immunol. 2017; 8

[212]. Sindrilaru A, Peters T, Wieschalka S, Baican C, Baican A, Peter H, Hainzl A, Schatz S, Qi Y, Schlecht A, Weiss JM, et al. An unrestrained proinflammatory M1 macrophage population induced by iron impairs wound healing in humans and mice. J Clin Invest. 2011; 121:985–997. [PubMed: 21317534]

[213]. Laskar A, Eilertsen J, Li W, Yuan X-M. SPION primes THP1 derived M2 macrophages towards M1-like macrophages. Biochem Biophys Res Commun. 2013; 441:737–742. [PubMed: 24184477]

[214]. Zanganeh S, Hutter G, Spitler R, Lenkov O, Mahmoudi M, Shaw A, Pajarinen JS, Nejadnik H, Goodman S, Moseley M, Coussens LM, et al. Iron oxide nanoparticles inhibit tumour growth by inducing pro-inflammatory macrophage polarization in tumour tissues. Nat Nanotechnol. 2016; 11:986–994. [PubMed: 27668795]

[215]. Vinchi F, Silva MCd, Ingoglia G, Petrillo S, Brinkman N, Zuercher A, Cerwenka A, Tolosano E, Muckenthaler MU. Hemopexin therapy reverts heme-induced proinflammatory phenotypic switching of macrophages in a mouse model of sickle cell disease. Blood. 2016; 127:473–486. [PubMed: 26675351]

[216]. Thiesen B, Jordan A. Clinical applications of magnetic nanoparticles for hyperthermia. Int J Hyperthermia. 2008; 24:467–474. [PubMed: 18608593]

[217]. Kumar CSSR, Mohammad F. Magnetic Nanomaterials for Hyperthermia-based Therapy and Controlled Drug Delivery. Adv Drug Deliv Rev. 2011; 63:789–808. [PubMed: 21447363]

[218]. Cole AJ, Yang VC, David AE. Cancer Theranostics: The Rise of Targeted Magnetic Nanoparticles. Trends Biotechnol. 2011; 29:323–332. [PubMed: 21489647]

[219]. Maier-Hauff K, Ulrich F, Nestler D, Niehoff H, Wust P, Thiesen B, Orawa H, Budach V, Jordan A. Efficacy and safety of intratumoral thermotherapy using magnetic iron-oxide nanoparticles combined with external beam radiotherapy on patients with recurrent glioblastoma multiforme. J Neurooncol. 2011; 103:317–324. [PubMed: 20845061]

[220]. Jordan A, Scholz R, Maier-Hauff K, van Landeghem FK, Waldoefner N, Teichgraeber U, Pinkernelle J, Bruhn H, Neumann F, Thiesen B. The effect of thermotherapy using magnetic nanoparticles on rat malignant glioma. J Neurooncol. 2006; 78:7–14. [PubMed: 16314937]

[221]. Attaluri A, Kandala SK, Wabler M, Zhou H, Cornejo C, Armour M, Hedayati M, Zhang Y, DeWeese TL, Herman C, Ivkov R. Magnetic nanoparticle hyperthermia enhances radiation therapy: A study in mouse models of human prostate cancer. International Journal of Hyperthermia. 2015; 31:359–374. [PubMed: 25811736]

[222]. Johannsen M, Gneveckow U, Thiesen B, Taymoorian K, Cho CH, Waldöfner N, Scholz R, Jordan A, Loening SA, Wust P. Thermotherapy of Prostate Cancer Using Magnetic Nanoparticles: Feasibility, Imaging, and Three-Dimensional Temperature Distribution. Eur Urol. 2007; 52:1653–1662. [PubMed: 17125906]

[223]. Stupp R, Hegi ME, Mason WP, van den Bent MJ, Taphoorn MJ, Janzer RC, Ludwin SK, Allgeier A, Fisher B, Belanger K, Hau P, et al. Effects of radiotherapy with concomitant and adjuvant temozolomide versus radiotherapy alone on survival in glioblastoma in a randomised phase III study: 5-year analysis of the EORTC-NCIC trial. Lancet Oncol. 2009; 10:459–466. [PubMed: 19269895]

[224]. Stupp R, Mason WP, van den Bent MJ, Weller M, Fisher B, Taphoorn MJ, Belanger K, Brandes AA, Marosi C, Bogdahn U, Curschmann J, et al. Radiotherapy plus concomitant and adjuvant temozolomide for glioblastoma. N Engl J Med. 2005; 352:987–996. [PubMed: 15758009]

[225]. Al-Jamal KT, Bai J, Wang JT, Protti A, Southern P, Bogart L, Heidari H, Li X, Cakebread A, Asker D, Al-Jamal WT, et al. Magnetic Drug Targeting: Preclinical in Vivo Studies, Mathematical Modeling, and Extrapolation to Humans. Nano Lett. 2016; 16:5652–5660. [PubMed: 27541372]

[226]. Schillinger U, Brill T, Rudolph C, Huth S, Gersting S, Krötz F, Hirschberger J, Bergemann C, Plank C. Advances in magnetofection—magnetically guided nucleic acid delivery. J Magn Magn Mater. 2005; 293:501–508.

[227]. Krötz F, De Wit C, Sohn H-Y, Zahler S, Gloe T, Pohl U, Plank C. Magnetofection—a highly efficient tool for antisense oligonucleotide delivery in vitro and in vivo. Mol Ther. 2003; 7:700–710. [PubMed: 12718913]

[228]. Thorek DL, Ulmert D, Diop N-FM, Lupu ME, Doran MG, Huang R, Abou DS, Larson SM, Grimm J. Non-invasive mapping of deep-tissue lymph nodes in live animals using a multimodal PET/MRI nanoparticle. Nature communications. 2014; 5:3097.

[229]. Polyak B, Friedman G. Magnetic targeting for site-specific drug delivery: applications and clinical potential. Expert Opin Drug Deliv. 2009; 6:53–70. [PubMed: 19236208]

[230]. Plank C, Anton M, Rudolph C, Rosenecker J, Krotz F. Enhancing and targeting nucleic acid delivery by magnetic force. Expert Opin Biol Ther. 2003; 3:745–758. [PubMed: 12880375]

[231]. Scherer F, Anton M, Schillinger U, Henke J, Bergemann C, Krüger A, Gänsbacher B, Plank C. Magnetofection: enhancing and targeting gene delivery by magnetic force in vitro and in vivo. Gene Ther. 2002; 9:102. [PubMed: 11857068]

[232]. Wilson MW, Kerlan RK, Fidelman NA, Venook AP, LaBerge JM, Koda J, Gordon RL. Hepatocellular Carcinoma: Regional Therapy with a Magnetic Targeted Carrier Bound to Doxorubicin in a Dual MR Imaging/ Conventional Angiography Suite—Initial Experience with Four Patients. Radiology. 2004; 230:287–293. [PubMed: 14695402]

[233]. Koda J, Venook A, Walser E, Goodwin S. A multicenter, phase I/II trial of hepatic intra-arterial delivery of doxorubicin hydrochloride adsorbed to Magnetic Targeted Carriers in patients with hepatocellular carcinoma. Eur Cancer J. 2002; 38:S18.

[234]. Miller MA, Arlauckas S, Weissleder R. Prediction of anti-cancer nanotherapy efficacy by imaging. Nanotheranostics. 2017; 1:296. [PubMed: 29071194]

[235]. Miller MA, Gadde S, Pfirschke C, Engblom C, Sprachman MM, Kohler RH, Yang KS, Laughney AM, Wojtkiewicz G, Kamaly N, Bhonagiri S, et al. Predicting therapeutic nanomedicine efficacy using a companion magnetic resonance imaging nanoparticle. Sci Transl Med. 2015; 7:314ra183–314ra183.

[236]. Ramanathan RK, Korn RL, Raghunand N, Sachdev JC, Newbold RG, Jameson G, Fetterly GJ, Prey J, Klinz SG, Kim J, Cain J, et al. Correlation between Ferumoxytol Uptake in Tumor Lesions by MRI and Response to Nanoliposomal Irinotecan in Patients with Advanced Solid Tumors: A Pilot Study. Clinical Cancer Research: An Official Journal of the American Association for Cancer Research. 2017; 23:3638–3648. [PubMed: 28159813]

[237]. El-Dakdouki MH, Xia J, Zhu DC, Kavunja H, Grieshaber J, O'Reilly S, McCormick JJ, Huang X. Assessing the in Vivo Efficacy of Doxorubicin Loaded Hyaluronan Nanoparticles. ACS Appl Mater Interfaces. 2014; 6:697–705. [PubMed: 24308364]

[238]. Li K, Nejadnik H, Daldrup-Link HE. Next-generation superparamagnetic iron oxide nanoparticles for cancer theranostics. Drug Today Discov. 2017; 22:1421–1429.

[239]. Medarova Z, Pham W, Farrar C, Petkova V, Moore A. In vivo imaging of siRNA delivery and silencing in tumors. Nat Med. 2007; 13:372. [PubMed: 17322898]

[240]. Kaittanis C, Bolaender A, Yoo B, Shah N, Ouerfelli O, Grimm J. Targetable Clinical Nanoparticles for Precision Cancer Therapy Based on Disease-Specific Molecular Inflection Points. Nano Lett. 2017; 17:7160–7168. [PubMed: 29035540]

[241]. Remsen LG, McCormick CI, Roman-Goldstein S, Nilaver G, Weissleder R, Bogdanov A, Hellström I, Kroll R, Neuwelt E. MR of carcinoma-specific monoclonal antibody conjugated to monocrystalline iron oxide nanoparticles: the potential for noninvasive diagnosis. American Journal of Neuroradiology. 1996; 17:411–418. [PubMed: 8881233]

[242]. Kumar M, Yigit M, Dai G, Moore A, Medarova Z. Image-guided breast tumor therapy using a small interfering RNA nanodrug. Cancer Res. 2010

[243]. Schleich N, Po C, Jacobs D, Ucakar B, Gallez B, Danhier F, Préat V. Comparison of active, passive and magnetic targeting to tumors of multifunctional paclitaxel/SPIO-loaded nanoparticles for tumor imaging and therapy. J Control Release. 2014; 194:82–91. [PubMed: 25178270]

[244]. Lammers T, Kiessling F, Hennink WE, Storm G. Nanotheranostics and image-guided drug delivery: current concepts and future directions. Mol Pharm. 2010; 7:1899–1912. [PubMed: 20822168]

[245]. Koczera P, Appold L, Shi Y, Liu M, Dasgupta A, Pathak V, Ojha T, Fokong S, Wu Z, Van Zandvoort M. PBCA-based polymeric microbubbles for molecular imaging and drug delivery. J Control Release. 2017; 259:128–135. [PubMed: 28279799]

[246]. Kiessling F, Fokong S, Bzyl J, Lederle W, Palmowski M, Lammers T. Recent advances in molecular, multimodal and theranostic ultrasound imaging. Adv Drug Deliv Rev. 2014; 72:15–27. [PubMed: 24316070]

[247]. Lammers T, Koczera P, Fokong S, Gremse F, Ehling J, Vogt M, Pich A, Storm G, van Zandvoort M, Kiessling F. Theranostic USPIO-Loaded Microbubbles for Mediating and Monitoring Blood-Brain Barrier Permeation. Adv Funct Mater. 2015; 25:36–43. [PubMed: 25729344]

[248]. Yang F, Zhang M, He W, Chen P, Cai X, Yang L, Gu N, Wu J. Controlled release of Fe3O4 nanoparticles in encapsulated microbubbles to tumor cells via sonoporation and associated cellular bioeffects. Small. 2011; 7:902–910. [PubMed: 21374806]

[249]. Cheung JS, Chow AM, Guo H, Wu EX. Microbubbles as a novel contrast agent for brain MRI. Neuroimage. 2009; 46:658–664. [PubMed: 19269337]

[250]. Sontum PC. Physicochemical characteristics of Sonazoid™, a new contrast agent for ultrasound imaging. Ultrasound Med Biol. 2008; 34:824–833. [PubMed: 18255220]

[251]. Klibanov AL. Ultrasound molecular imaging with targeted microbubble contrast agents. J Nucl Cardiol. 2007; 14:876. [PubMed: 18022115]

[252]. Chen Y-C, Jiang L-P, Liu N-X, Wang Z-H, Hong K, Zhang Q-P. P85, Optison microbubbles and ultrasound cooperate in mediating plasmid DNA transfection in mouse skeletal muscles in vivo. Ultrason Sonochem. 2011; 18:513–519. [PubMed: 20863738]

[253]. Cooley M, Jung O, Exner AA. Ultrasound Contrast Agents and Delivery Systems in Cancer Detection and Therapy. Cancer Nanotechnol. 2018; 139:57.

[254]. Liu HL, Hsu PH, Chu PC, Wai YY, Chen JC, Shen CR, Yen TC, Wang JJ. Magnetic resonance imaging enhanced by superparamagnetic iron oxide particles: Usefulness for distinguishing between focused ultrasound-induced blood–brain barrier disruption and brain hemorrhage. Journal of Magnetic Resonance Imaging: An Official Journal of the International Society for Magnetic Resonance in Medicine. 2009; 29:31–38.

[255]. Fan C-H, Ting C-Y, Lin H-J, Wang C-H, Liu H-L, Yen T-C, Yeh C-K. SPIO-conjugated, doxorubicin-loaded microbubbles for concurrent MRI and focused-ultrasound enhanced brain-tumor drug delivery. Biomaterials. 2013; 34:3706–3715. [PubMed: 23433776]

[256]. Liu G, Wang Z, Lu J, Xia C, Gao F, Gong Q, Song B, Zhao X, Shuai X, Chen X, Ai H, et al. Low molecular weight alkyl-polycation wrapped magnetite nanoparticle clusters as MRI probes for stem cell labeling and in vivo imaging. Biomaterials. 2011; 32:528–537. [PubMed: 20869767]

[257]. Mertens ME, Hermann A, Bühren A, Olde-Damink L, Möckel D, Gremse F, Ehling J, Kiessling F, Lammers T. Iron Oxide-labeled Collagen Scaffolds for Non-invasive MR Imaging in Tissue Engineering. Adv Funct Mater. 2014; 24:754–762. [PubMed: 24569840]

[258]. Mertens ME, Koch S, Schuster P, Wehner J, Wu Z, Gremse F, Schulz V, Rongen L, Wolf F, Frese J, Gesché VN, et al. USPIO-labeled textile materials for non-invasive MR imaging of tissue-engineered vascular grafts. Biomaterials. 2015; 39:155–163. [PubMed: 25465443]

[259]. Kircher MF, Allport JR, Graves EE, Love V, Josephson L, Lichtman AH, Weissleder R. In vivo high resolution three-dimensional imaging of antigen-specific cytotoxic T-lymphocyte trafficking to tumors. Cancer Res. 2003; 63:6838–6846. [PubMed: 14583481]

[260]. Budde MD, Frank JA. Magnetic tagging of therapeutic cells for MRI. J Nucl Med. 2009; 50

[261]. Cho N-H, Cheong T-C, Min JH, Wu JH, Lee SJ, Kim D, Yang J-S, Kim S, Kim YK, Seong S-Y. A multifunctional core–shell nanoparticle for dendritic cell-based cancer immunotherapy. Nat Nanotechnol. 2011; 6:675. [PubMed: 21909083]

[262]. Perica K, Tu A, Richter A, Bieler JG, Edidin M, Schneck JP. Magnetic field-induced T cell receptor clustering by nanoparticles enhances T cell activation and stimulates antitumor activity. ACS Nano. 2014; 8:2252–2260. [PubMed: 24564881]

[263]. Toraya-Brown S, Sheen MR, Zhang P, Chen L, Baird JR, Demidenko E, Turk MJ, Hoopes PJ, Conejo-Garcia JR, Fiering S. Local hyperthermia treatment of tumors induces CD8+ T cell-mediated resistance against distal and secondary tumors. World Scientific. 2016; 3:309–347.

[264]. Jasmin, n; de Souza, GT; Louzada, RA; Rosado-de-Castro, PH; Mendez-Otero, R; Campos de Carvalho, AC. Tracking stem cells with superparamagnetic iron oxide nanoparticles: perspectives and considerations. Int J Nanomedicine. 2017; 12:779–793. [PubMed: 28182122]

[265]. Bull E, Madani SY, Sheth R, Seifalian A, Green M, Seifalian AM. Stem cell tracking using iron oxide nanoparticles. Int J Nanomedicine. 2014; 9:1641–1653. [PubMed: 24729700]

[266]. Feo DD, Merlini A, Laterza C, Martino G. Neural stem cell transplantation in central nervous system disorders: from cell replacement to neuroprotection. Curr Opin Neurol. 2012; 25:322–333. [PubMed: 22547103]

[267]. Saudek F, Jirák D, Girman P, Herynek V, Dezortová M, Kríz J, Peregrin J, Berková Z, Zacharovova K, Hajek M. Magnetic resonance imaging of pancreatic islets transplanted into the liver in humans. Transplantation. 2010; 90:1602–1606. [PubMed: 21197715]



Europe PMC Funders Author Manuscripts

Europe PMC Funders Author Manuscripts

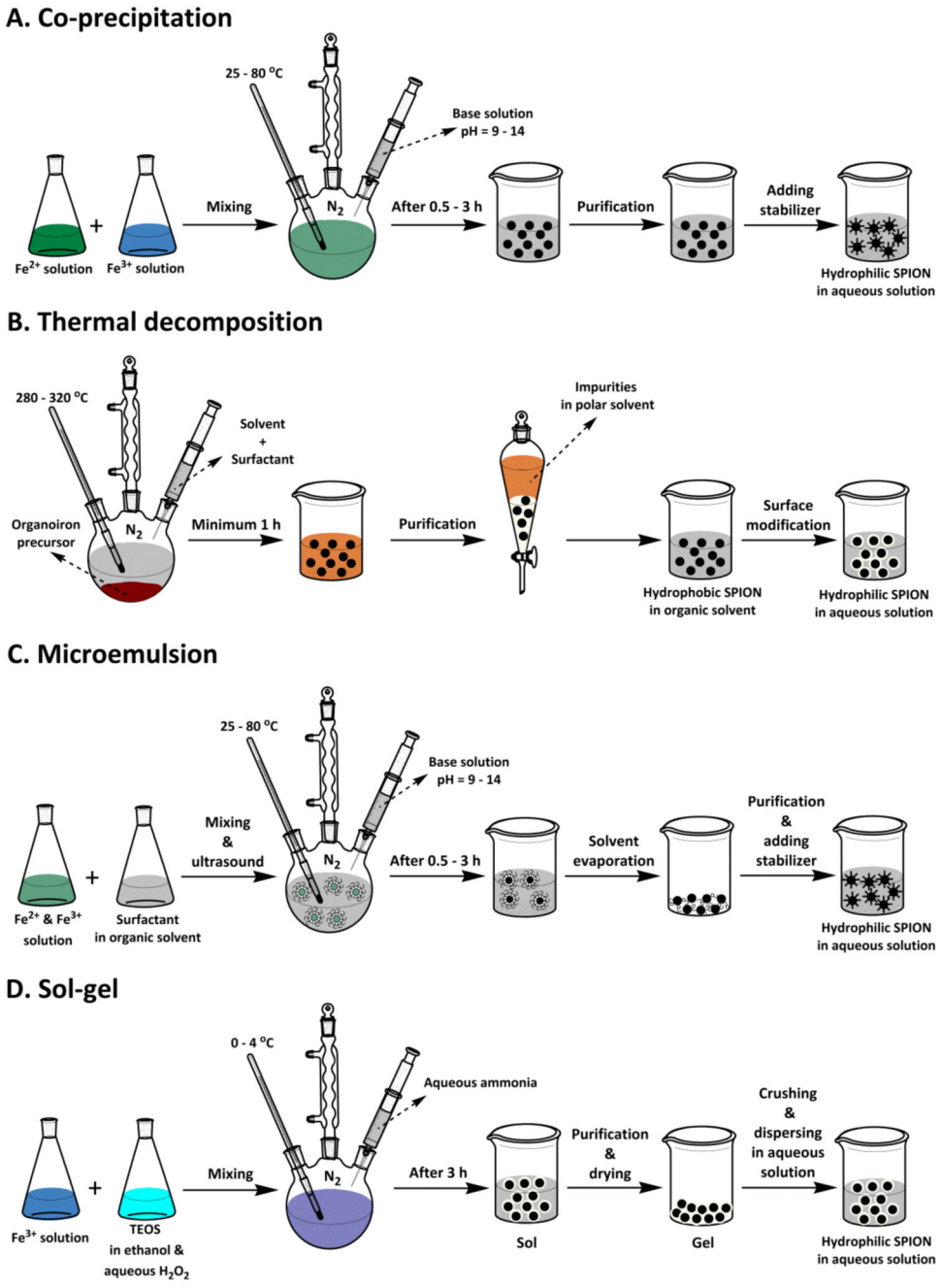


**Figure 1. Schematic depiction of commonly used chemical strategies to prepare iron oxide nanoparticles.**

A: Co-precipitation, B: Thermal decomposition, C: Micro-emulsion and D: Sol-gel. In terms of simplicity, the co-precipitation technique is the most suitable. In terms of size and morphology control, and for producing SPION smaller than 20 nm, thermal decomposition and microemulsion are preferred. The sol-gel technique is useful to produce SPION with silica coatings and with a size larger than 20 nm.

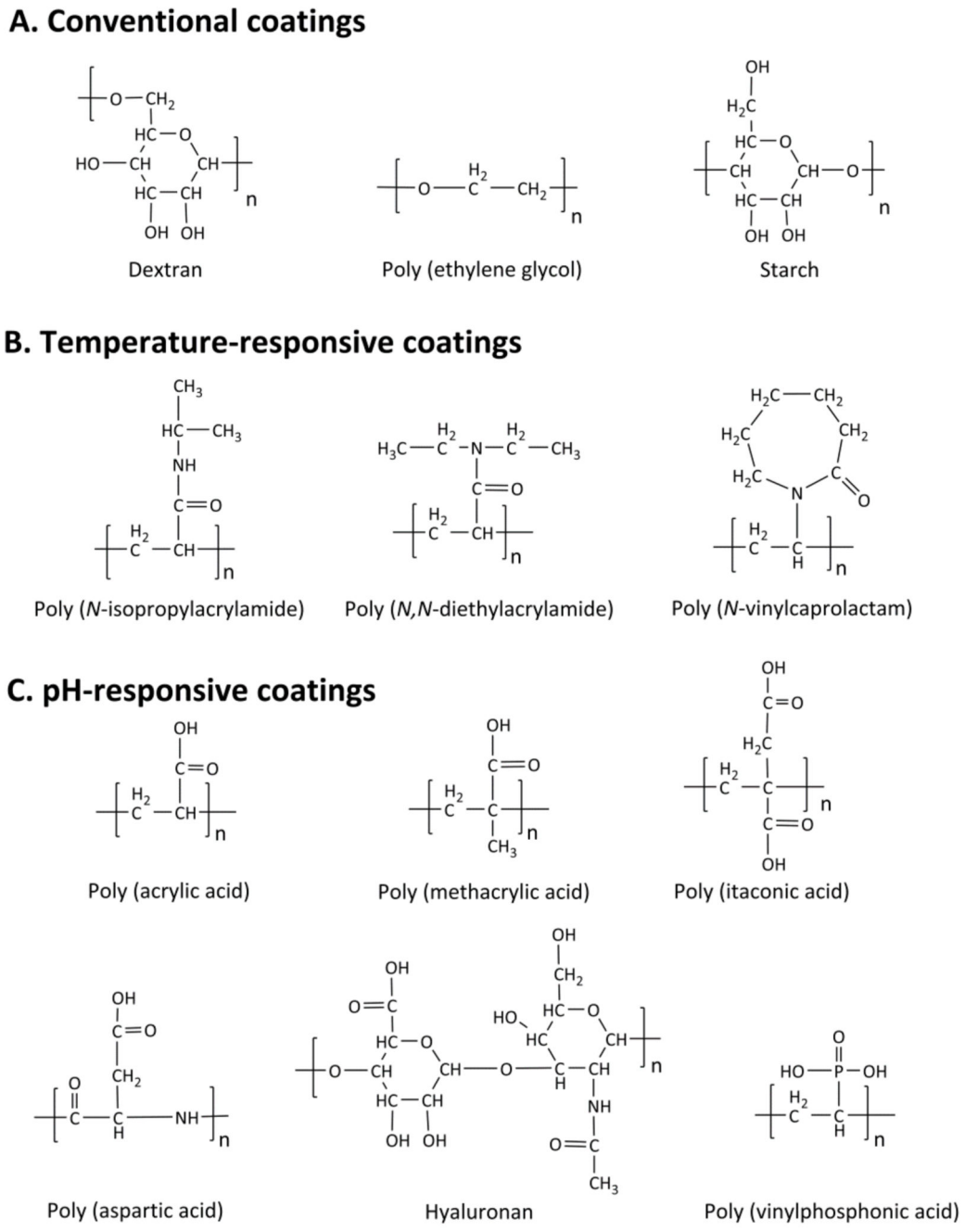


**Figure 2. Examples of polymers used as surface coatings of iron oxide nanoparticles.**

Conventional polymers (A) are used as coatings in the commercial iron oxide nanoparticle formulations listed in Table 1. For certain applications, iron oxide nanoparticles are surface-functionalized with temperature (B) or pH (C) -responsive polymeric coating.

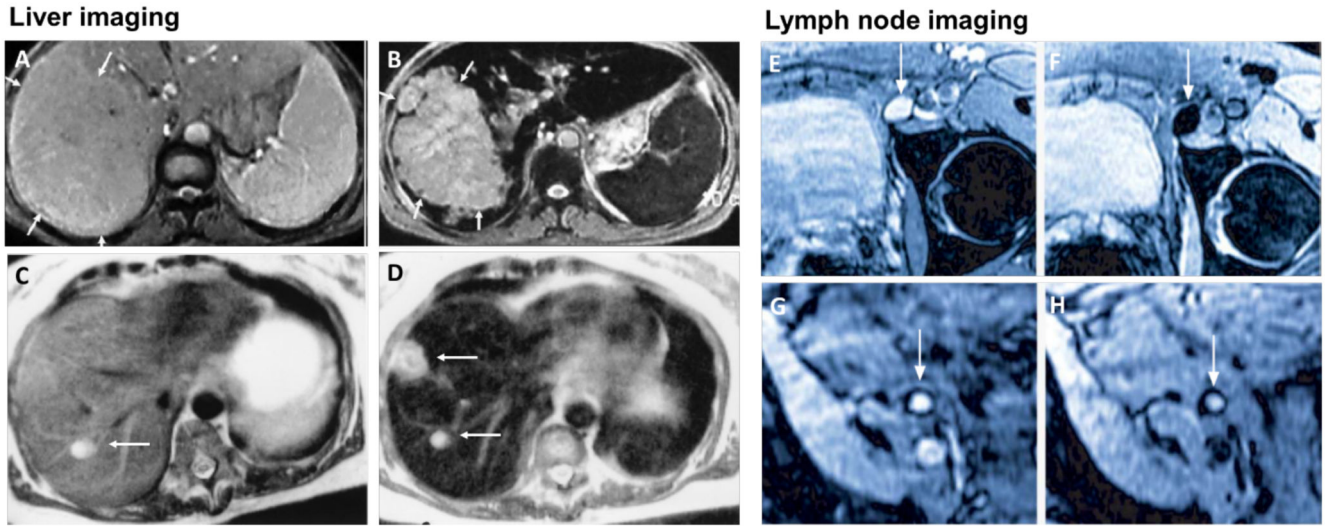


**Figure 3. SPION for liver imaging and lymph node imaging.**

A-B: T2-weighted MR image of a liver with a large hepatocellular carcinoma before (A) and after (B) the administration of SPION. The lesion is demarcated with arrows [168]. C-D: Standard (C) and SPION-based contrast-enhanced (D) MR imaging of liver metastasis in a patient with colorectal cancer. After administration of ferumoxide SPION, a second metastasis becomes visible on T2-weighted MR image [148]. E-H: Lymph node in left iliac region (arrow), with and without metastatic infiltration. T2-weighted images before (E, G) and 24 h after (F, H) administration of ferumoxtran. Lymph node (arrow) appears bright before injection of UPIO (E, G). One day after injection, a signal loss in the lymph node (arrow) due to high UPIO macrophage uptake can be observed, thus indicating functionality and no metastasis (F). Conversely, in the lower panel, the lymph node (arrow) stays bright, indicating no trafficking of USPIO and thus metastatic colonization (H) [161].

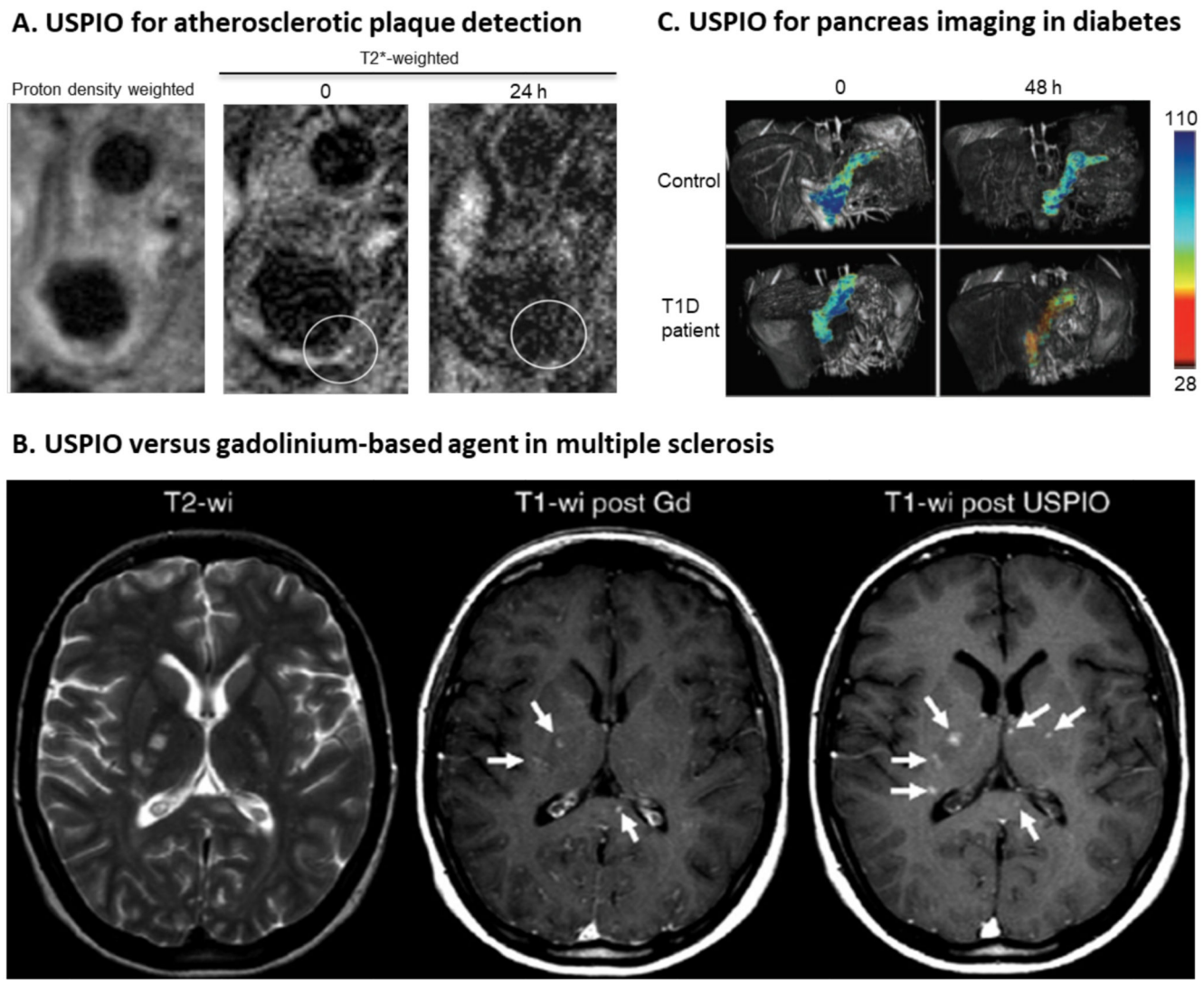


**Figure 4. Imaging inflammation with USPIO nanoparticles.**

A: MR images of external and internal carotid artery in a patient with atherosclerosis. T2*-weighted MR images before (middle) and 24 h after (right) the intravenous administration of USPIO nanoparticles. Around the vessel wall (circle) a decrease in signal intensity can be observed [172] B: Differences in enhancement pattern between USPIO nanoparticles and gadolinium-based MRI contrast agents in a patient suffering from multiple sclerosis (MS). Left, multiple hyperintense lesions can be detected on the non-contrast-enhanced T2-weighted image. Middle, gadolinium-based T1-weighted image showing three contrast-enhanced MS lesions (arrows). USPIO with core diameter smaller than 4 nm show shortening of T1 relaxation and therefore have been used for T1-weighted images. Right, T1-weighted image obtained after USPIO administration, showing the same three lesions and three additional lesions (arrows), exemplifying the added value of iron oxide-based diagnostic assessment in MS [175]. C: T2-based pseudocolor MR images showing enhanced SPION accumulation in a T1D diabetic patient as compared to a healthy individual [178].

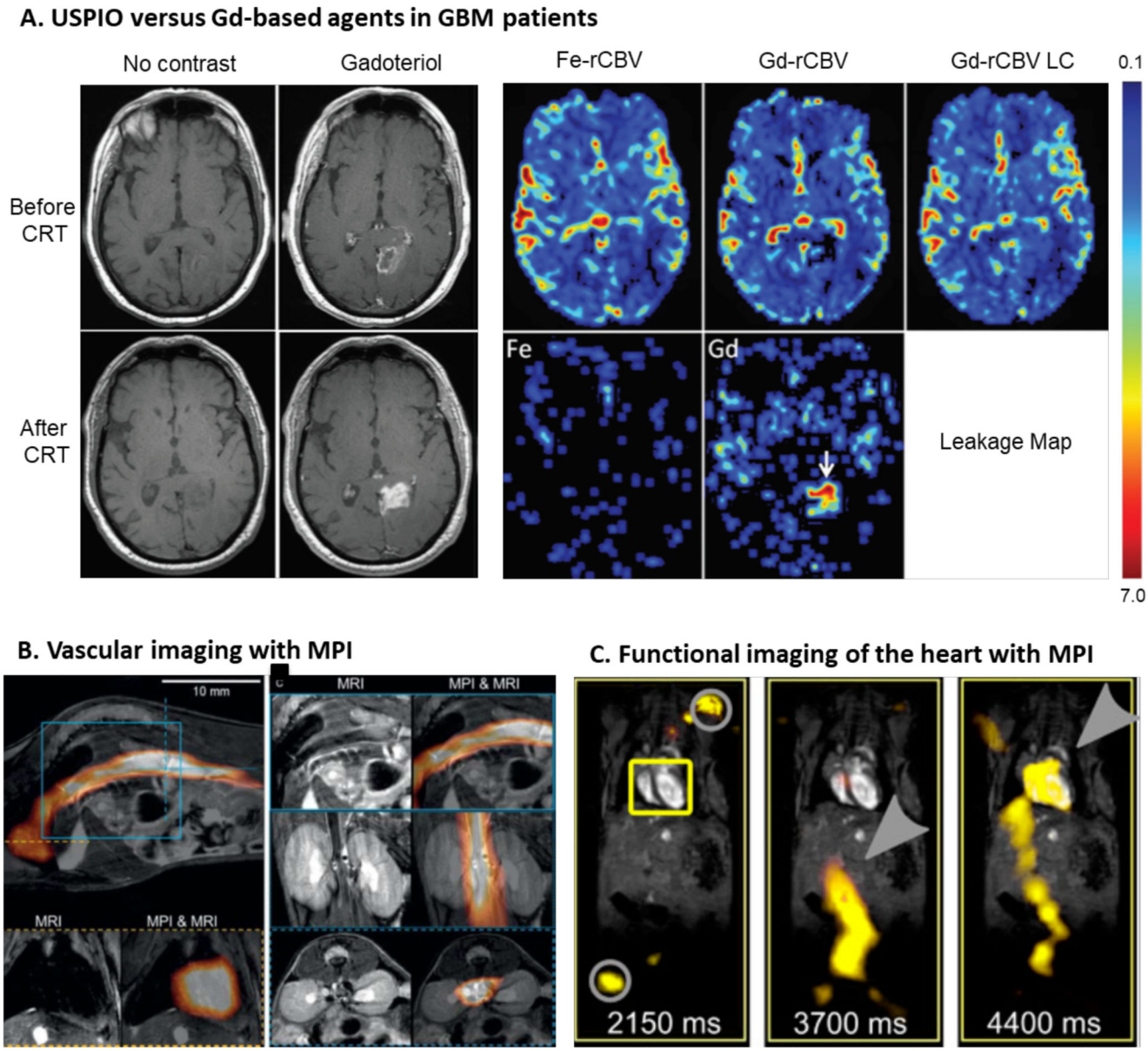


**Figure 5. Iron oxide nanoparticles for vascular imaging.**

[184]. A: Non-contrast-enhanced and gadolinium-enhanced Tl-weighted MR images before and after chemoradiotherapy (CRT) show an increase in hyperintensity in the lesion, indicative of (pseudo-) progression. Relative cerebral blood volume (rCBV) evaluated with ferumoxytol (Fe-rCBV), gadoteridol (Gd-rCBV) and gadoteridol with leakage correction (Gd-rCBV LC) all show low rCBV, which identifies this situation as pseudoprogression. The leakage map shows contrast agent accumulation for gadoteridol (arrow), while no leakage is observed for ferumoxytol [191]. B: Images combining magnetic particle imaging (MPI) with MRI. Circulating ferucarbotran-based SPION are visualized by MPI, while MRI provides anatomical information. Bottom left images show SPION circulating through the heart. The top images and bottom right images show SPION in the inferior vena cava (sagittal, coronal

and transverse orientation, respectively) [194]. C: In vivo measurement from a beating mouse heart by MRI and overlaid with traveling wave MPI data. At 2150 m after the i.v. injection ferucarbotran-based SPION, no signal can be detected in the heart (yellow box), only the signal of the marker points for co-registration (grey circle) is detectable. At 3700 ms, the SPION can be seen in the artery that is leading to the heart (grey arrow), and after 4400 ms, the SPION eventually reaches the heart (grey arrow). [195].

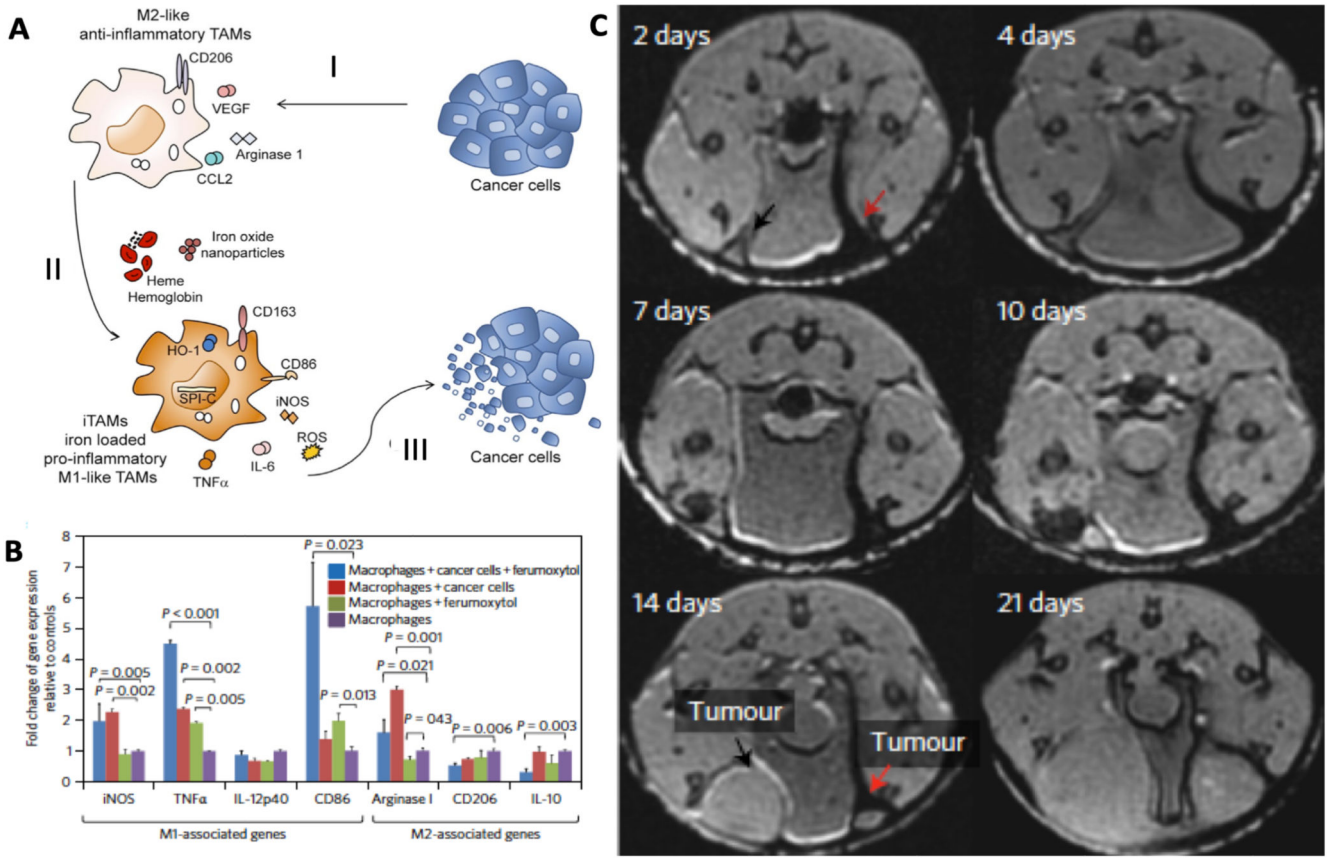


**Figure 6. Iron oxide nanoparticles alter macrophage polarization towards an anti-tumoral phenotype.**

A. SPION or hemoglobin induce a shift in activation of tumor growth supporting TAM to a more M1-like anti-tumoral phenotype. I. Tumor cells support M2-like polarization by inducing a variety of growth factors and receptors like CCL2, VEGF or cluster of differentiation 206 (CD206). II. TAM exposed to SPION or hemoglobin change their polarization towards a pro-inflammatory phenotype with high generation of TNFα, IL-6 and ROS. III. Iron-loaded TAM show an anti-tumoral activity and decrease the viability of cancer cells [211]. B. Polarization of macrophages induced by ferumoxytol. PCR results show a significant increase in the expression of typical M1 markers like TNFα for the iron oxide nanoparticle-treated group compared to untreated. C. Co-injection of SPION (ferumoxtran or ferumoxytol) with MMTV-PyMT derived cancer cells into the mammary fat pad of mice showed a significant inhibition of tumor growth in comparison to the non-SPION containing controls. T2*-weighted MR images on day 2 shows SPION-related darkening (red arrow) which is absent on the side which was only injected with cancer cells. On day 14 after tumor cell inoculation, MRI shows a growth inhibitory effect for ferumoxytol co-injection (red arrow) as compared to controls (black arrow) [214].




Europe PMC Funders Author Manuscripts

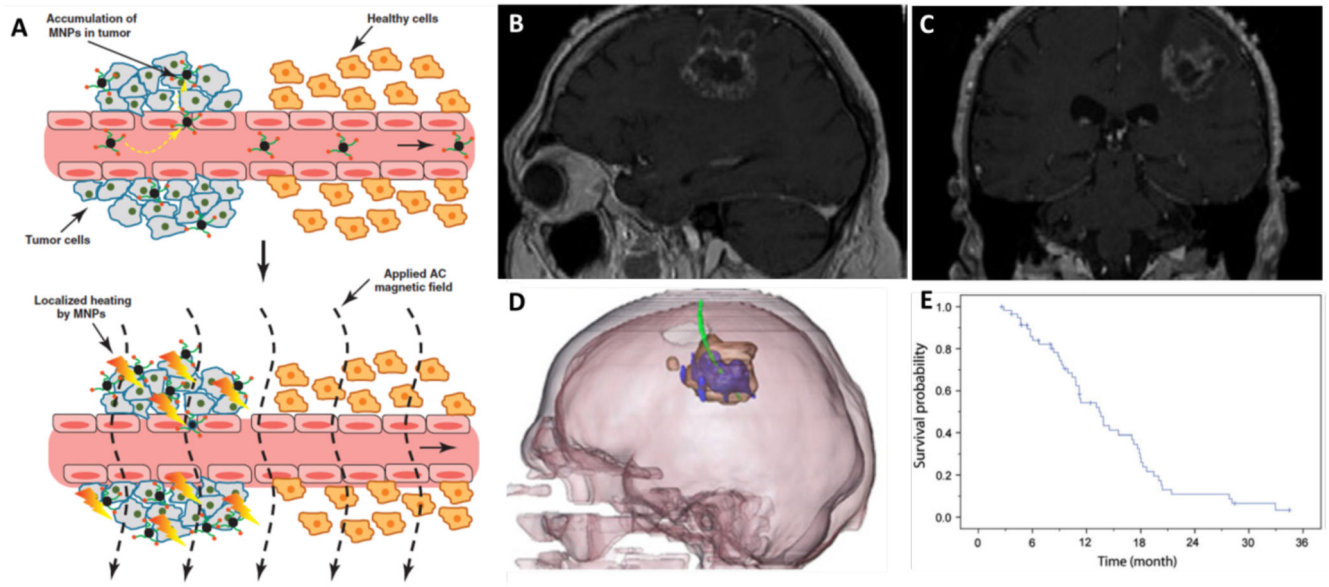


**Figure 7. Magnetic drug targeting and magnetic fluid hyperthermia.**

A. Schematic depiction of magnetic fluid hyperthermia mechanism of action. The upper image shows the specific accumulation of magnetic nanoparticles (MNP) in tumor tissue due to leaky vasculature (EPR). The lower image exemplifies that after the application of an alternating current (AC) magnetic field, the SPION which have accumulated in the tumor heat up and lead to tissue damage [218]. B-C. MR images of patients with recurrent GBM before treatment. D. Fusion of MRI and CT (3D-reconstruction) shows the thermometry catheter in green, magnetic fluid in blue and glioblastoma tumor mass in brown. E. Overall survival of 59 glioblastoma patients after diagnosis of first tumor recurrence and treatment with combination of magnetic fluid hyperthermia and radiotherapy [219].




Europe PMC Funders Author Manuscripts

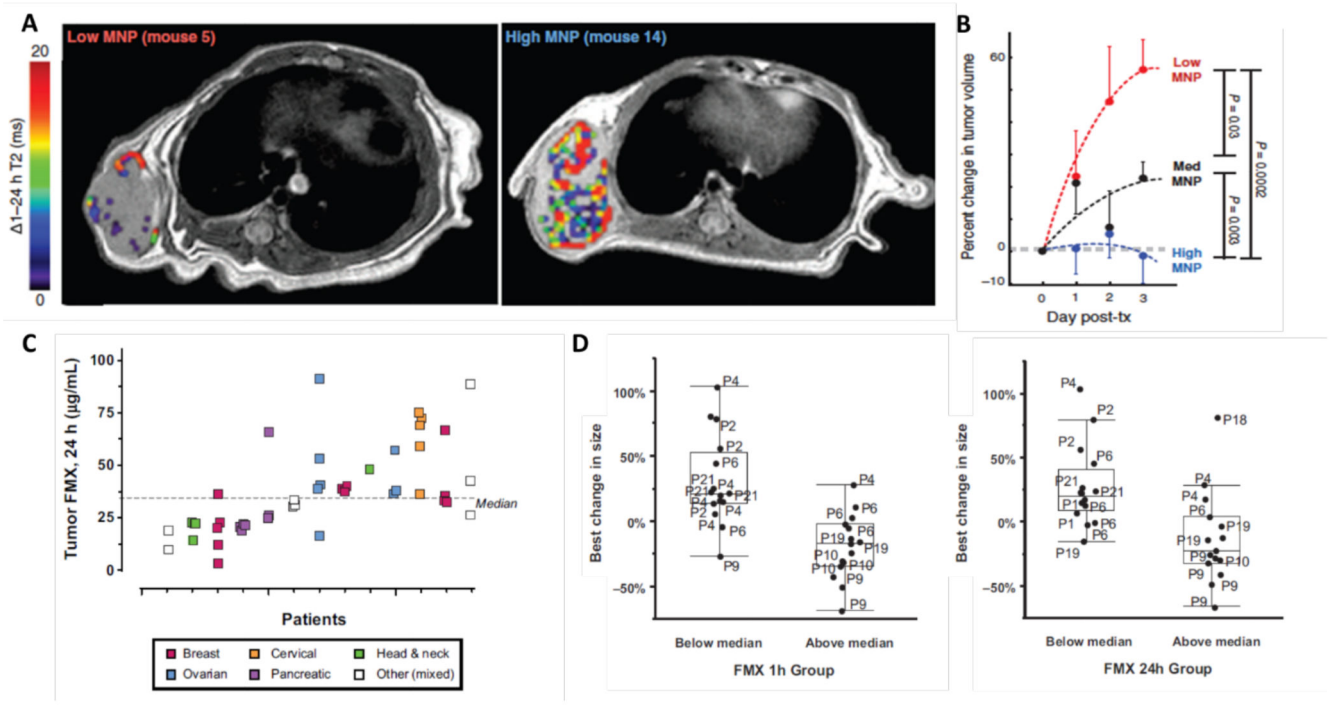


**Figure 8. Iron oxide-based companion diagnostics.**

A: T2-weigthed MR images (overlaid with pseudocolor images indicating ΔT2 in the tumor area) show varying levels of accumulation of ferumoxytol-based iron oxide nanoparticles in HT1080 tumors in mice. Low and high magnetic nanoparticle (MNP) corresponds to tumors with low and high levels of tumor targeting. B: Correlation between the tumor accumulation of iron oxide-based companion diagnostics and the antitumor response progression induced by paclitaxel-loaded PLGA-PEG nanoparticles [235]. C: Ferumoxytol concentration in different tumor lesions at 24 h after i.v. injection, showing highly heterogeneous uptake in individual lesions. D: Correlation between lesion size change after treatment with irinotecan-loaded liposomes determined by CT measurements on the one hand, and ferumoxytol uptake in the different lesions detected by MRI at 1 h and 24 h after injection on the other hand. For every time point, the median tumor accumulation of ferumoxytol was calculated. Based on this, the lesions were classified in below vs. above the median, and this was correlated with irinotecan-loaded liposome treatment efficacy. A decent correlation between ferumoxytol uptake and lesion size change was observed [236].

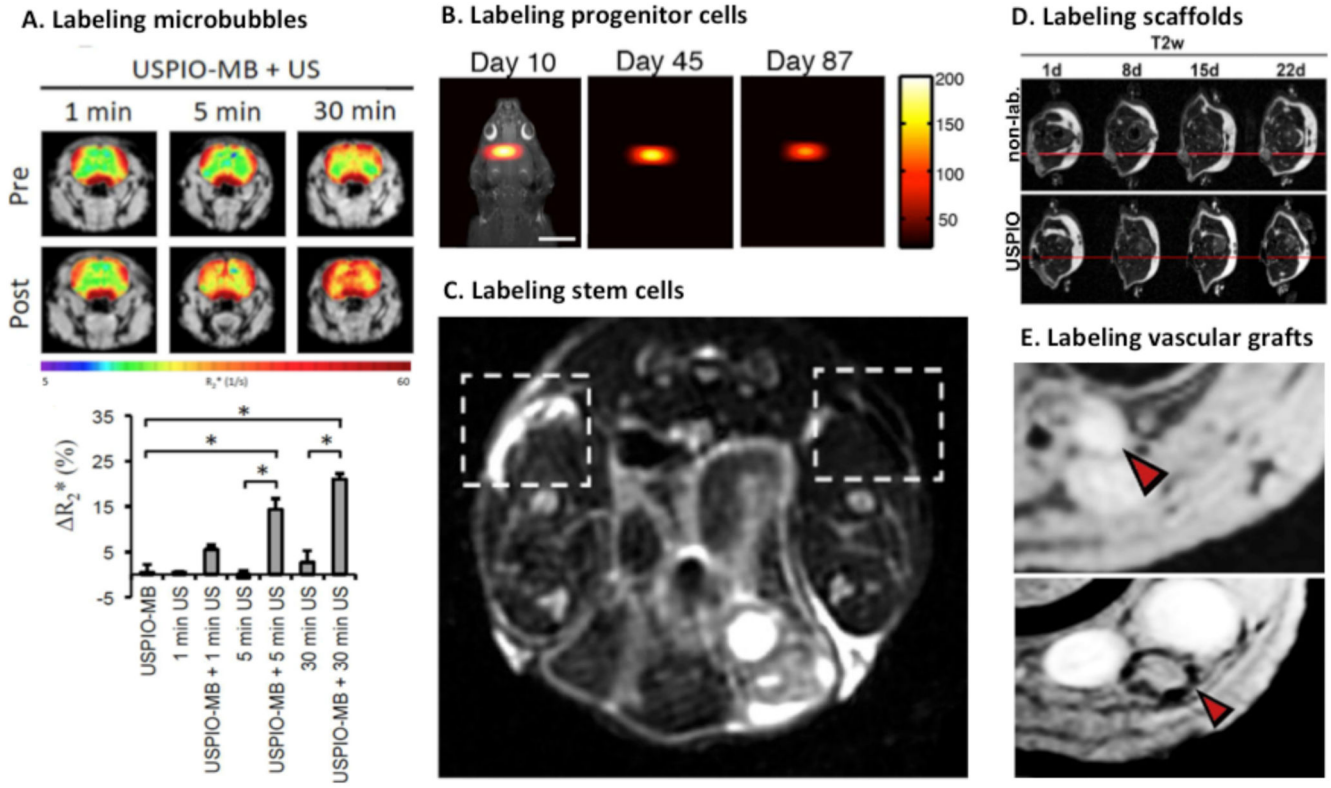


**Figure 9. Theranostic applications of iron oxide nanoparticles in brain drug delivery and in regenerative medicine.**

A: Permeation of the blood-brain barrier (BBB), induced and imaged using microbubbles of which the shell was loaded with iron oxide nanoparticles (USPIO-MB). Upper panel: T2*-weighted images overlaid with color-coded R*-maps, showing ultrasound-induced destruction of USPIO-MB, BBB opening and the subsequent deposition of iron oxide nanoparticles in the brain. Lower panel: Quantification of R2* values shows gradual enhancement of BBB opening when increasing the time of ultrasound exposure [247]. B: Tracing of ferucarbotran-labeled human neuronal progenitor cells with MPI in the forebrain cortex of rats [198]. C: SPION-labeled mesenchymal stem cells (MSC) in collagen-based hydrogels 19 days after implantation, visualized using MRI. T2*-weighted image shows hypointense region on right side compared to the unlabeled control implanted on left side. [256]. D: Unlabeled (upper) and USPIO-labeled (lower) collagen scaffolds implanted in mice, showing clear dark areas in T2-weighted MRI in case of iron oxide nanoparticle labeling [257]. E: Tissue-engineered vascular grafts implanted as a shunt between the carotid artery and the jugular vein in sheep can be clearly visualized using proton density-weighted MRI when iron oxide nanoparticles are integrated (compare lower vs. upper panel) [258].




Europe PMC Funders Author Manuscripts

## Table 1

**Examples of iron oxide nanoparticles approved or in clinical trials.**

| Generic name | Trade name | Short name | Coating | Relaxivity* | $D_h$ † | $D_c$ # | Applications | Clinical trial | Clinically approved |
|---|---|---|---|---|---|---|---|---|---|
| Ferumoxtran | Combidex® (USA) Sinerem® (EU) | AMI-227 | Dextran | $r_1$ = 9.9 $r_2$ = 65 | 15 - 30 | 5.9 | lymph node imaging, macrophage imaging, blood pool agent, cell labeling, CNS imaging | ✓ | |
| Ferucarbotran Ferrixan | Resovist® (USA, Japan, EU) Cliavist® (France) | SHU-555A | Carboxydextran | $r_1$ = 9.7 $r_2$ = 189 | 62 | 4 | liver imaging, CNS imaging, cell labeling | | ✓‡ |
| Ferumoxide | Feridex I.V. (USA) Endorem™ (EU) | AMI-25 | Dextran | $r_1$ = 10.1 $r_2$ = 120 | 120 - 180 | 5 | liver imaging, CNS imaging, cell labeling | | ✓× |
| Ferumoxytol | Feraheme® (USA) Rienso® (EU) | Code 7228 | Carboxymethyl-dextran | $r_1$ = 15 $r_2$ = 89 | 17 - 31 | n.a. | iron replacement therapy in patients with chronic kidney failure, CNS imaging, macrophage imaging, blood pool agent, cellular labeling, lymph node imaging | | ✓+ |
| Feruglose | Clariscan™ | NC100150 | PEGylated starch | n.a. | 20 | n.a. | blood pool agent | ✓ | |
| Ferumoxsil | Lumirem® (USA) GastroMARK® (EU) | AMI-121 | Siloxane | $r_1$ = 2 $r_2$ = 47 | 300 | 8.4 | oral GI imaging | | ✓× |
| | Abdoscan® | - | Sulfonated poly(styrene-divinylbenzene) copolymer | n.a. | 3500 | n.a. | oral GI imaging | | ✓ |

*Relaxometric properties ($mM^{-1}.s^{-1}$) at 1.5 T, at 37 °C and in water or plasma.

†$D_h$: hydrodynamic diameter, in nm, determined by laser light scattering.

#$D_C$: core size diameter, in nm, determined by transmission electron microscopy.

‡Available in only limited countries.

×withdrawn from the market.

+withdrawn from EU market

CNS: central nervous system.
GI: gastrointestinal.
n.a.: not available.

Europe PMC Funders Author Manuscripts

**Table 2**

**Summary comparison of different SPION synthesis method.**

| Method | Synthesis procedure | Process temperature | Process time | Size distribution | Shape control | Morphology | Degree of crystallinity | Yield | Scalable |
|---|---|---|---|---|---|---|---|---|---|
| Coprecipitation | Very simple | Low | Minutes | Broad | Bad | Irregular sphere | Low | High | Yes |
| Thermal decomposition | Very Complicated | High | Hours-days | Vary narrow | Very good | Cube-sphere | High | High | Yes |
| Microemulsion | Complicated | Low | Hours | Relatively narrow | Good | Cube-sphere | Low | Low | No |
| Sol-gel | Relatively simple | Low | Hours | Relatively narrow | Good | Porous or nonporous sphere | Low | Medium | Yes |
| Hydrothermal | Relatively simple | High | Hours | Relatively Broad | Bad | Irregular sphere | High | Medium | Yes |
| Sonochemical decomposition | Complicated | Low (locally very high) | Minutes | Narrow | Bad | Bipyramid-rod-sphere | low | Medium | No |
| Electrochemical deposition | Relatively simple | Low | Hours | Relatively narrow | Bad | Rod-sphere-hexagonal | low | Medium | No |

Europe PMC Funders Author Manuscripts

## Table 3
**Key studies applying SPION in diagnosis, therapy and theranostics.**

| Field of application | Application | Indication | Product | Phase | Ref |
|---|---|---|---|---|---|
| Diagnosis | Lymph node staging, detection of small metastatic lymph nodes | Prostate cnacer | Ferumoxtran | Phase II | [157] |
| | Magnetic nanoparticle-based biosensors (DMR - diagnostic magnetic resonance) for detection of biomarkers | Cancer, inflammation | Surface modified CLIO | Market | [205] |
| Therapy | Iron supplement for anemic patients | Chronic kidney disease | Ferumoxytol | Market | [209] |
| | Magnetic fluid hyperthermia | Recurrent glioblastoma multiforme | NanoTherm® | Market | [220] |
| Theranostics | Companion diagnostics, evaluate accumulation and predict treatment efficacy of nanomedical cancer therapy | Cancer | Ferumoxytol | Pilot study | [236] |
| | Tagging of dendritic cell, injected intranodally and employed for immune system stimulation | Melanoma | Ferumoxide | Phase I | [126] |

CLIO - cross linked iron oxide